Twenty Years of Generalized Barycentric Coordinates

Jiong Chen
Inria
30/03/2026 @ BUF

Useful Resources

- https://www.inf.usi.ch/hormann/barycentric/

Barycentric Coordinates

Welcome to the **Barycentric Coordinates** homepage! This website follows our minisymposia given at the 10th SIAM Conference on Geometric Design & Computing and the 2011 SIAM Conference on Geometric & Physical Modeling. It provides links to online resources, including slides and papers.

Contributors

- Mirela Ben-Chen, Stanford University
- Solveig Bruvoll, University of Oslo
- Michael S. Floater, University of Oslo
- Andrew Gillette, University of California, San Diego
- Kai Hormann, University of Lugano
- Tao Ju, Washington University
- Jiří Kosinka, University of Cambridge
- Raif Rustamov, Drew University
- Scott Schaefer, Texas A&M University
- N. Sukumar, UC Davis

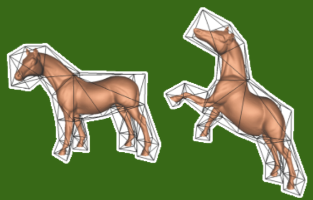

Slides

Minisymposium on **Barycentric Coordinates and Transfinite Interpolation**

- Lecture 1: Generalized Barycentric Coordinates by Kai Hormann
- Lecture 2: Barycentric Coordinates for Closed Curves by Scott Schaefer
- Lecture 3: Hermite Mean Value Interpolation by Michael S. Floater
- Lecture 4: A General, Geometric Construction of Coordinates in any Dimensions by Tao Ju
- Lecture 5: Transfinite Mean Value Interpolation over Volumetric Domains by Solveig Bruvoll
- Lecture 6: Barycentric Finite Element Methods by N. Sukumar

Minisymposium on **Theory and Applications of Barycentric Coordinates**

- Lecture 1: Constructing Barycentric Coordinates on Surfaces by Raif Rustamov
- Lecture 2: Injective Barycentric Mappings on Convex Domains by Jiří Kosinka
- Lecture 3: Geometric Criteria for Generalized Barycentric Finite Elements by Andrew Gillette
- Lecture 4: Variational Space Deformations with Barycentric Coordinates by Mirela Ben-Chen

Keynote Lecture on Generalized Barycentric Coordinates by Kai Hormann

Papers

before 1900

- Der barycentrische Calcul
  August F. Möbius, 1827

before 2000

- Continuity and convexity of projections and barycentric coordinates in convex polyhedra
  John A. Kalman, 1961
- A rational basis for function approximation
  Eugene L. Wachspress, 1971
- A rational basis for function approximation. II: Curved sides
  Eugene L. Wachspress, 1973
- Pseudo-harmonic interpolation on convex domains
  William J. Gordon and James A. Wixom, 1974
- A Rational Finite Element Basis
  Eugene L. Wachspress, 1975
- Rational basis functions for curved elements
  Eugene L. Wachspress, 1979
- High-order curved finite elements
  Eugene L. Wachspress, 1981
- A pentagonal surface patch for computer aided geometric design
  Peter Charrot and John A. Gregory, 1984
- A multisided generalization of Bézier surfaces
  Charles T. Loop and Tony D. DeRose, 1989
- Computing discrete minimal surfaces and their conjugates
  Ulrich Pinkall and Konrad Polthier, 1993
- Multiresolution analysis of arbitrary meshes
  Matthias Eck, Tony DeRose, Tom Duchamp, Hugues Hoppe, Michael Lounsbery, and Werner Stuetzle, 1995
- Barycentric coordinates for convex polytopes
  Joe Warren, 1996

Prof. Kai Hormann

Useful Resources

Book

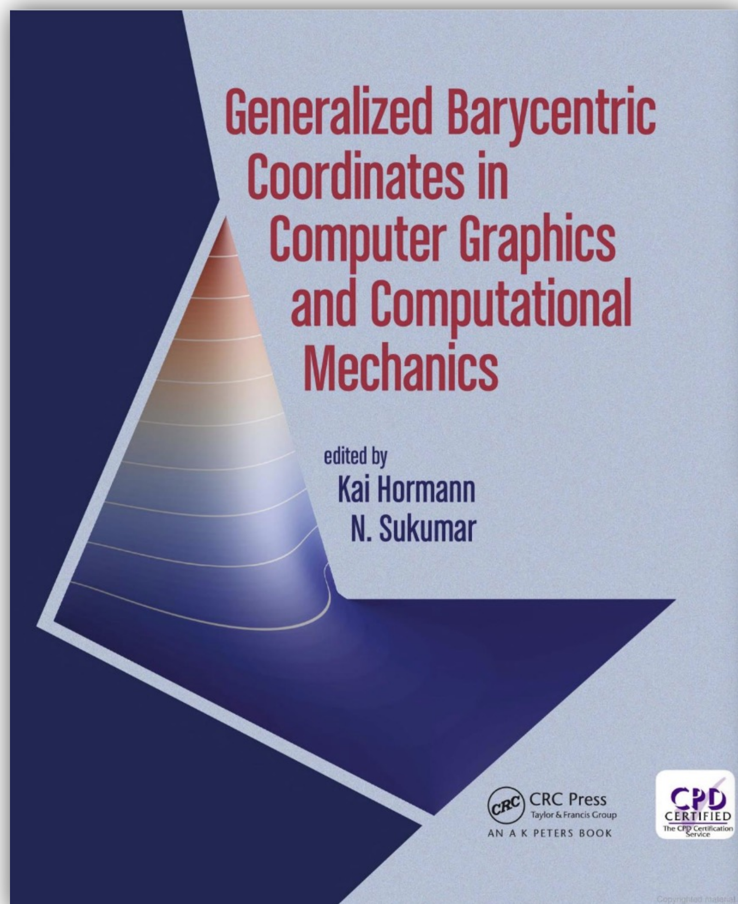

Survey papers

Acta Numerica (2016), pp. 001–
doi:10.1017/S09624929

Generalized barycentric coordinates and applications

Michael S. Floater
Department of Mathematics,
University of Oslo,
P.O. Box 1053 Blindern, 0316 Oslo, Norway
E-mail: michaelf@ifi.uio.no

EUROGRAPHICS 2024
A. Aristidou and R. McDonnell
(Guest Editors)
COMPUTER GRAPHICS *forum*
Volume 43 (2024), Number 2
STAR – State of The Art Report

A Survey on Cage-based Deformation of 3D Models

D. Ströter[1], J. M. Thiery[2], K. Hormann[3], J. Chen[4], Q. Chang[3], S. Besler[1,5], J. S. Mueller-Roemer[1,5], T. Boubekeur[2], A. Stork[1,5] and D. W. Fellner[1,5,6]
[1]Technical University of Darmstadt, Germany [2]Adobe Research, France [3]Università della Svizzera italiana, Lugano, Switzerland [4]Inria, France [5]Fraunhofer IGD, Germany [6]Graz University of Technology, Institute of Computer Graphics and Knowledge Visualization, Austria

Barycentric Coordinates

- Express a point $x \in \Omega$ with the vertices of a simplex
  - e.g., a triangle, a tetrahedron
- Barycentric coordinates λ_i form linear combination of vertices p_i
- For a triangle: $x = \lambda_0 p_0 + \lambda_1 p_1 + \lambda_2 p_2$
- Partition of unity:

$$1 = \sum_{i=0}^{2} \lambda_i$$

- Solving for λ_i for point within a simplex

$$\begin{pmatrix} \lambda_0 \\ \lambda_1 \\ \lambda_2 \end{pmatrix} \begin{pmatrix} p_{0x} & p_{1x} & p_{2x} \\ p_{0y} & p_{1y} & p_{2y} \\ p_{0z} & p_{1z} & p_{2z} \end{pmatrix} = x$$

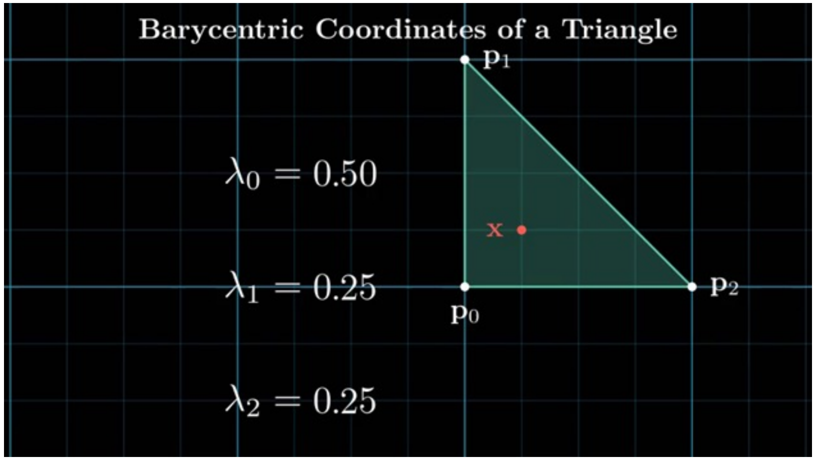

Generalized Barycentric Coordinates (GBC)

- GBC generalizes barycentric coordinates to non-simplicial shapes

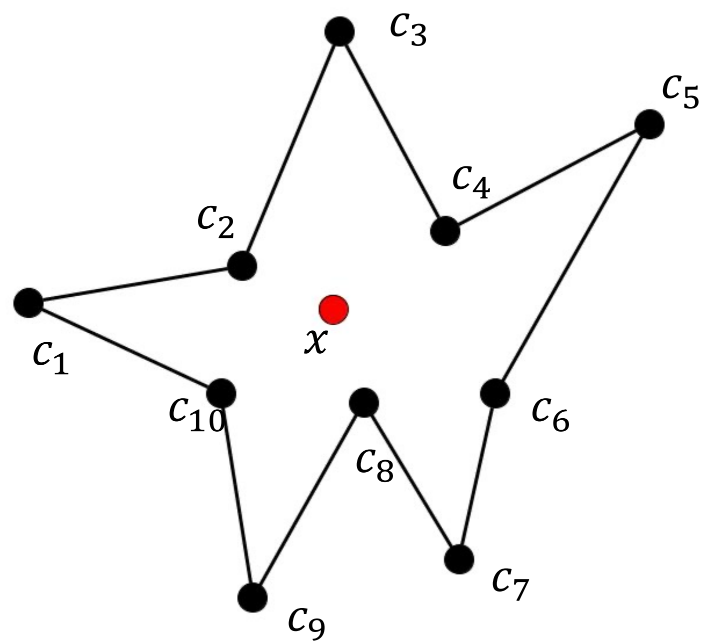

Generalized Barycentric Coordinates (GBC)

- GBC generalizes barycentric coordinates to non-simplicial shapes
- GBC is a set of functions $\lambda_i: \mathbb{R}^3 \rightarrow \mathbb{R}$
- Each function λ_i is associated with a vertex c_i
- Typically, solutions are not unique
  - Therefore, a large space to explore, and publish:)

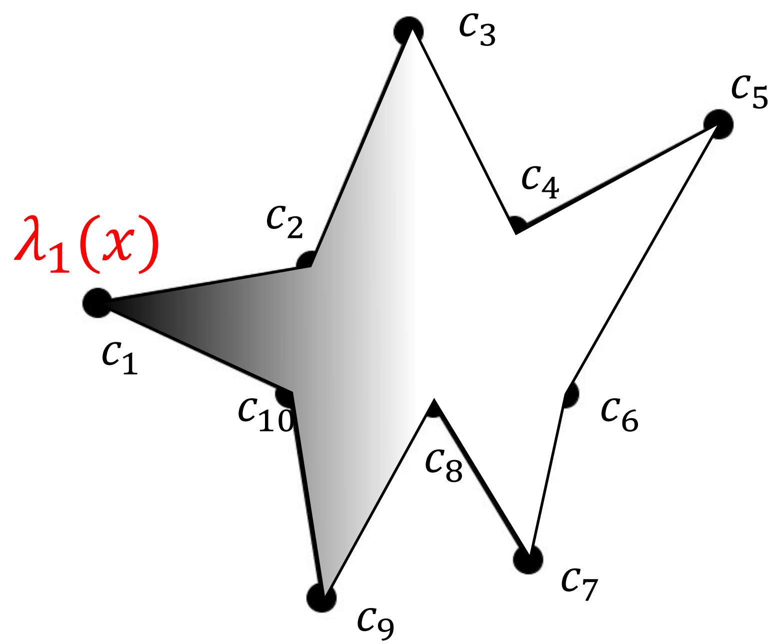

Cage Deformation

- Offline precomputation
  - Find GBC for N_C cage vertices c_i:

$$\sum_{i=1}^{N_C} \lambda_i(x) c_i = x$$

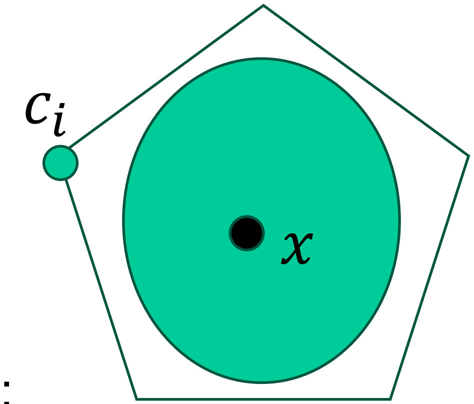

- Online computation
  - As the cage deforms, the interior mesh can be posed:

$$\sum_{i=1}^{N_C} \lambda_i(x) c_i' = x'$$

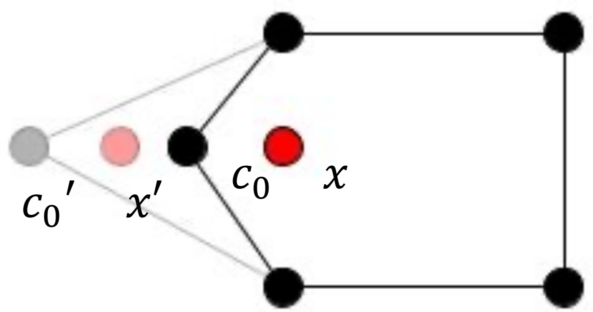

- In a matrix form

$$\begin{pmatrix} \lambda_{11} & \cdots & \lambda_{1N_C} \\ \vdots & \ddots & \vdots \\ \lambda_{N_V 1} & \cdots & \lambda_{N_V N_C} \end{pmatrix} \begin{pmatrix} c'_1 \\ \vdots \\ c'_{N_C} \end{pmatrix} = \begin{pmatrix} x_1' \\ \vdots \\ x_{N_V}' \end{pmatrix}$$

Precomputed, (#cage_verts, #mesh_verts)

What are good GBC?

- Partition of unity
  - $\sum_i \lambda_i(x) = 1, \forall x \in \Omega$
- Reproduction
  - $\sum_i \lambda_i(x) c_i = x, \forall x \in \Omega$
- Lagrange property
  - $\lambda_i(c_j) = \delta_{ij}$
  - Mesh follows cage tightly
- Non-negativity
  - $\lambda_i(x) \geq 0$
- Smoothness
  - $\lambda_i \in C^\infty$
- Locality
  - λ_i only influences regions nearby c_j
- Easy to compute
  - Pointwise evaluation based on closed-form expressions
  - No need to solve linear systems or optimizations

Linear precision

$$f(x) = Ax + b = A(\sum_i \lambda_i c_i) + b(\sum_i \lambda_i) = \sum_i \lambda_i (Ac_i + b) = \sum_i \lambda_i f(c_i)$$

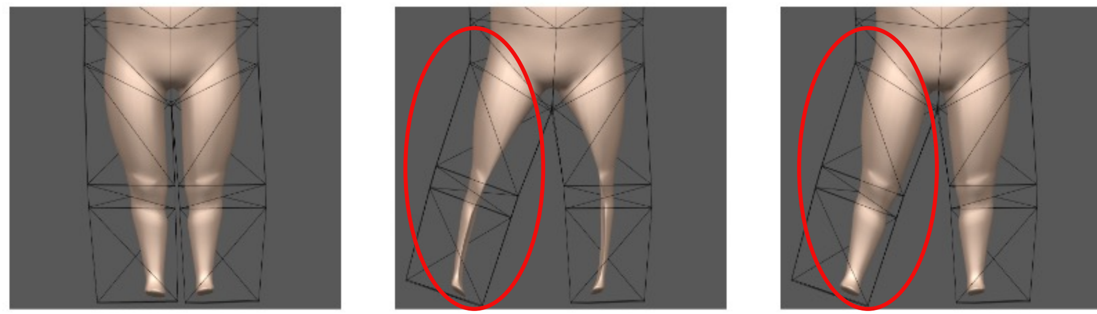

undeformed   negative (MVC)   non-negative (HC)

[JMD*07]

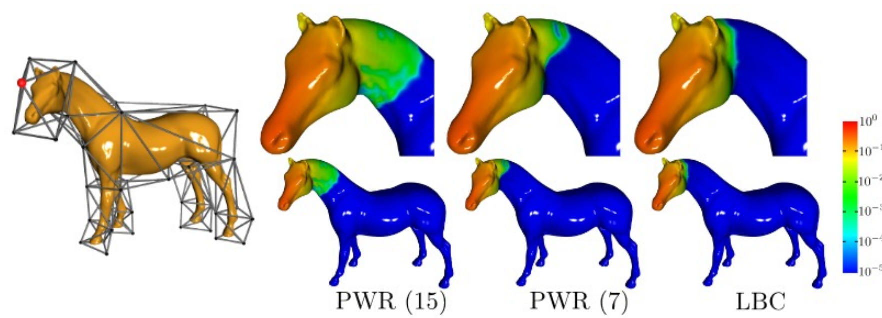

[ZDL*14]

A Brief History of GBC

- Barycentric coordinates for simplices (1827):
  - Möbius discovered that any point inside a triangle can be expressed as a unique, weighted sum of the triangle's three vertices (where the weights sum to 1).

August Möbius

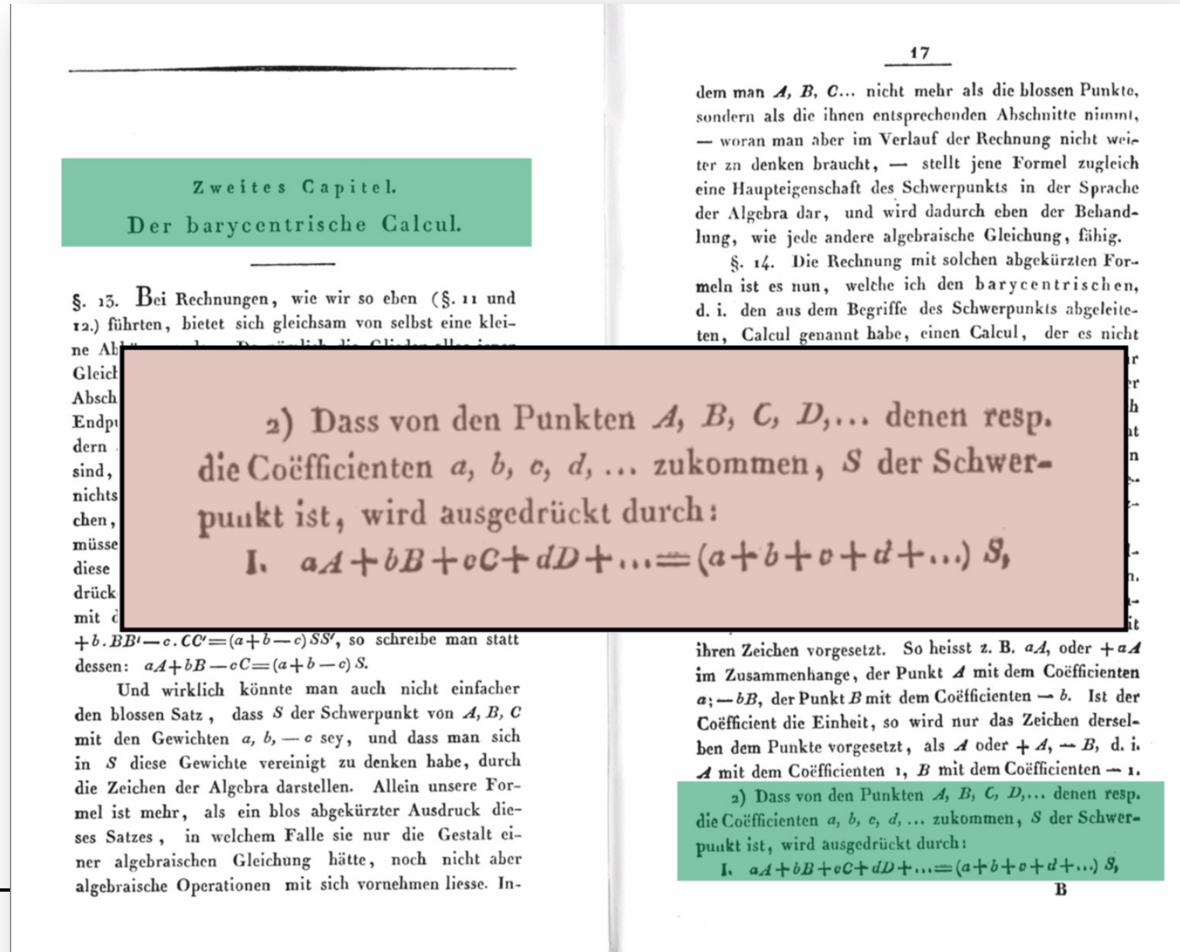

Zweites Capitel.

Der barycentrische Calcul.

§. 13. Bei Rechnungen, wie wir so eben (§. 11 und 12.) führten, bietet sich gleichsam von selbst eine kleine Ab[…] Gleich[…] Absch[…] Endp[…] dern […] sind, […] nichts […] chen, […] müsse[…] diese […] drück[…] mit […] $+b.BB'-c.CC'=(a+b-c)SS'$, so schreibe man statt dessen: $aA+bB-cC=(a+b-c)S$.

Und wirklich könnte man auch nicht einfacher den blossen Satz, dass S der Schwerpunkt von A, B, C mit den Gewichten $a, b, -c$ sey, und dass man sich in S diese Gewichte vereinigt zu denken habe, durch die Zeichen der Algebra darstellen. Allein unsere Formel ist mehr, als ein blos abgekürzter Ausdruck dieses Satzes, in welchem Falle sie nur die Gestalt einer algebraischen Gleichung hätte, noch nicht aber algebraische Operationen mit sich vornehmen liesse. In-

17

dem man $A, B, C\ldots$ nicht mehr als die blossen Punkte, sondern als die ihnen entsprechenden Abschnitte nimmt, — woran man aber im Verlauf der Rechnung nicht weiter zu denken braucht, — stellt jene Formel zugleich eine Haupteigenschaft des Schwerpunkts in der Sprache der Algebra dar, und wird dadurch eben der Behandlung, wie jede andere algebraische Gleichung, fähig.

§. 14. Die Rechnung mit solchen abgekürzten Formeln ist es nun, welche ich den barycentrischen, d. i. den aus dem Begriffe des Schwerpunkts abgeleiteten, Calcul genannt habe, einen Calcul, der es nicht […]

2) Dass von den Punkten $A, B, C, D,\ldots$ denen resp. die Coëfficienten $a, b, c, d, \ldots$ zukommen, S der Schwerpunkt ist, wird ausgedrückt durch:

I. $aA+bB+cC+dD+\ldots=(a+b+c+d+\ldots)S$,

[…] ihren Zeichen vorgesetzt. So heisst z. B. aA, oder $+aA$ im Zusammenhange, der Punkt A mit dem Coëfficienten a; $-bB$, der Punkt B mit dem Coëfficienten $-b$. Ist der Coëfficient die Einheit, so wird nur das Zeichen derselben dem Punkte vorgesetzt, als A oder $+A$, $-B$, d. i. A mit dem Coëfficienten 1, B mit dem Coëfficienten -1.

2) Dass von den Punkten $A, B, C, D,\ldots$ denen resp. die Coëfficienten $a, b, c, d, \ldots$ zukommen, S der Schwerpunkt ist, wird ausgedrückt durch:

I. $aA+bB+cC+dD+\ldots=(a+b+c+d+\ldots)S$,

B

A Brief History of GBC

- Wachspress Coordinates (1975):
  - Eugene Wachspress formulated the first true GBCs for polygons.
  - But, polygons are required to be convex

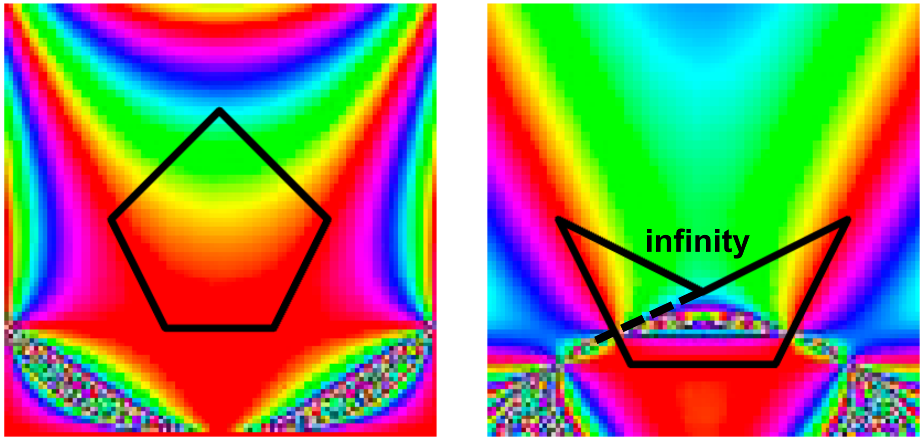

$$w_i(p) = \frac{cot(\alpha_{i-1}) + cot(\beta_i)}{\|p_i - p\|}$$

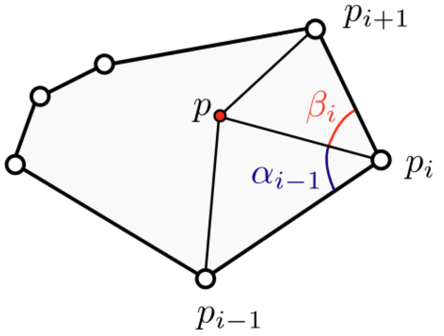

A Brief History of GBC

- Wachspress Coordinates (1975):
  - Eugene Wachspress formulated the first true GBCs for polygons.
  - But, polygons are required to be convex

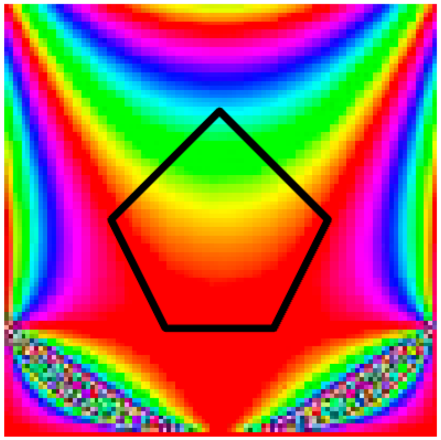

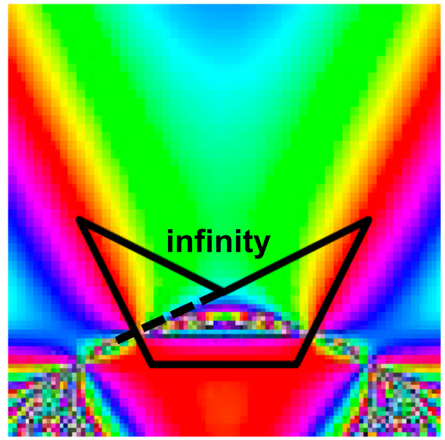

$$w_i(p) = \frac{cot(\alpha_{i-1}) + cot(\beta_i)}{\|p_i - p\|}$$

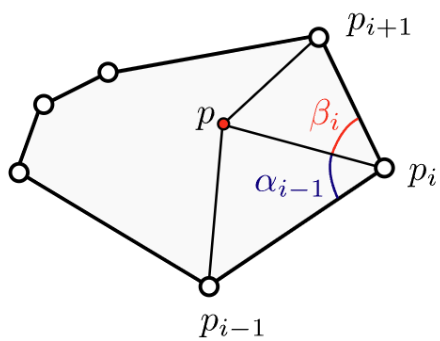

- Dealing with non-convex shapes (since early 2000s):
  - Mean value coordinates [Floater 2003; Ju et al. 2006]
  - Harmonic coordinates [Joshi et al. 2007]
  - Green coordinates [Lipman et al. 2008]
  - Cauchy coordinates [Weber et al. 2009]
  - ….

How to publish a GBC paper

- A machinery to interpolate from boundary
  - Mean value theorem of harmonic functions [Floater 2003; Ju et al. 2006]
  - Cauchy integral formula [Weber et al. 2009]
  - Green's third identity [Lipman et al. 2008]
  - Somigliana identity [Chen et al. 2023]
  - Boundary constrained harmonic equation [Joshi et al. 2007]
- Discretizing cage surface
  - Line segments (2D)
  - Triangles (3D)
  - Quads (3D)
  - Polygons (3D)
- Selecting basis functions
  - Piecewise linear functions
  - High-order polynomials

$$u(x) = \frac{1}{4\pi r^2} \iint_{\partial B(x,r)} u(y)\, dS(y)$$

$$f(a) = \frac{1}{2\pi i} \oint_\gamma \frac{f(z)}{z-a}\, dz$$

$$u(x) = \int_{\partial\Omega} \left[\Phi(y-x)\frac{\partial u}{\partial n}(y) - u(y)\frac{\partial \Phi}{\partial n}(y)\right] dS(y)$$

$$u_i(\xi) = \int_{\partial\Omega} [u^*_{ij}(x,\xi)t_j(x) - t^*_{ij}(x,\xi)u_j(x)]\, dS(x)$$

$$\Delta\phi_i(x) = 0, \quad x \in \Omega \quad \text{subject to } \phi_i(v_j) = \delta_{ij}$$

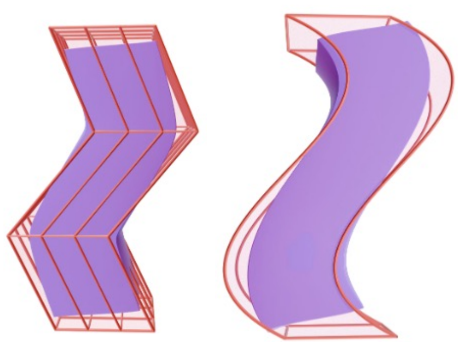

How to publish a GBC paper

$$\lambda_i(x) = \int_{\partial\Omega} \kappa(x,y)\Gamma_i(y)\, dy$$

$$u(x) = \frac{1}{4\pi r^2} \iint_{\partial B(x,r)} u(y)\, dS(y)$$

$$f(a) = \frac{1}{2\pi i} \oint_\gamma \frac{f(z)}{z-a}\, dz$$

- Green's third identity [
- Somigliana identity [C
- Boundary constrained
  [Joshi et al. 2007]

$$\lambda_i(x) = \mathrm{argmin}_f \; E\big(\nabla f(x)\big),$$
$$\text{s.t. linear precision, Lagrange property} \dots$$

- Discretizing cage surface
  - Line segments (2D)
  - Triangles (3D)
  - Quads (3D)
  - Polygons (3D)
- Selecting basis functions
  - Piecewise linear functions
  - High-order polynomials

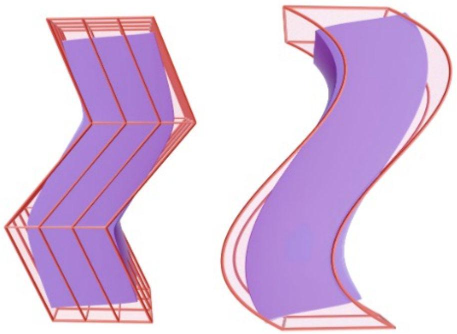

How to publish a GBC paper

$$\lambda_i(x) = \int_{\partial\Omega} \kappa(x,y)\Gamma_i(y)\, dy$$

$$u(x) = \frac{1}{4\pi r^2} \iint_{\partial B(x,r)} u(y)\, dS(y)$$

$$f(a) = \frac{1}{2\pi i} \oint_\gamma \frac{f(z)}{z-a}\, dz$$

- Green's third identity [
- Somigliana identity [C
- Boundary constrained
  [Joshi et al. 2007]

$$\lambda_i(x) = \mathrm{argmin}_f\, E\big(\nabla f(x)\big),$$
$$\text{s.t. linear precision, Lagrange property} \ldots$$

- Discretizing cage surface
  - Line segments (2D)
  - Triangles (3D)
  - Quads (3D)
  - Polygons (3D)
- Selecting basis functions
  - Piecewise linear functions
  - High-order polynomials

Generalized Barycentric Coordinates on Irregular Polygons

Mean value coordinates for quad cages in 3D

Green Coordinates for Triquad Cages in 3D

JEAN-MARC THIERY, Adobe Research, France
TAMY BOUBEKEUR, Adobe Research, France

Cubic Mean Value Coordinates

Polynomial 2D Biharmonic Coordinates for High-order Cages

Polynomial 2D Green Coordinates for Polygonal Cages

Special Section on CAD/Graphics 2025

Polynomial 3D Green coordinates and their derivatives for linear cages

Variational Green and Biharmonic Coordinates for 2D Polynomial Cages

ÉLIE MICHEL, Adobe Research, France

Polynomial Cauchy Coordinates for Curved Cages

Flexible 3D Cage-based Deformation via Green Coordinates on Bézier Patches

DONG XIAO, University of Science and Technology of China, China
RENJIE CHEN*, University of Science and Technology of China, China

GBC with closed-form expressions (Mean Value Coordinates)

Mean Value Coordinates (MVC)

- **Computing MVC in 2D [Floater 2003]**

Proposition 1. *The weights*

$$\lambda_i = \frac{w_i}{\sum_{j=1}^{k} w_j}, \qquad w_i = \frac{\tan(\alpha_{i-1}/2) + \tan(\alpha_i/2)}{\|v_i - v_0\|},$$

are coordinates for v_0 with respect to $v_1, \ldots, v_k$.

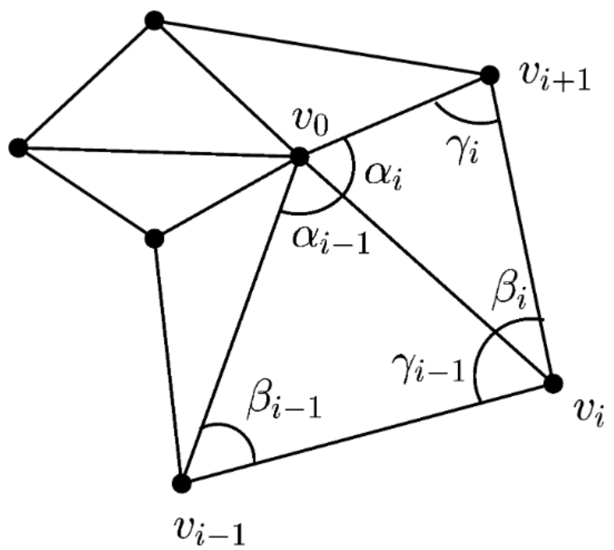

Fig. 1. Star-shaped polygon.

Mean Value Coordinates (MVC)

- **Computing MVC in 2D [Floater 2003]**

Proposition 1. *The*

$$\lambda_i = \frac{w_i}{\sum_{j=1}^{k} w_j}$$

are coordinates for

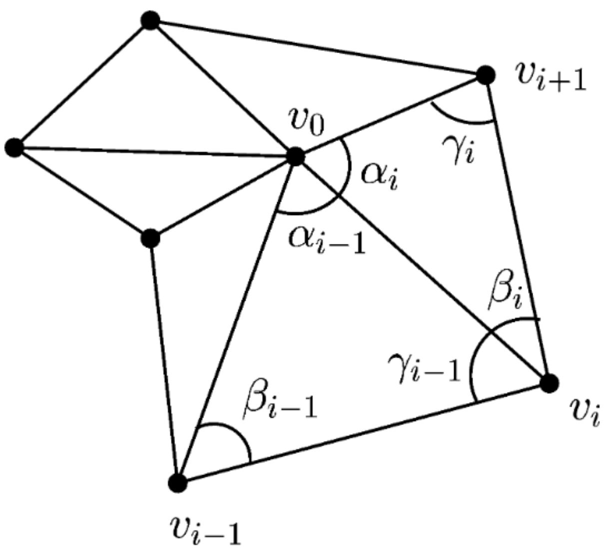

Fig. 1. Star-shaped polygon.

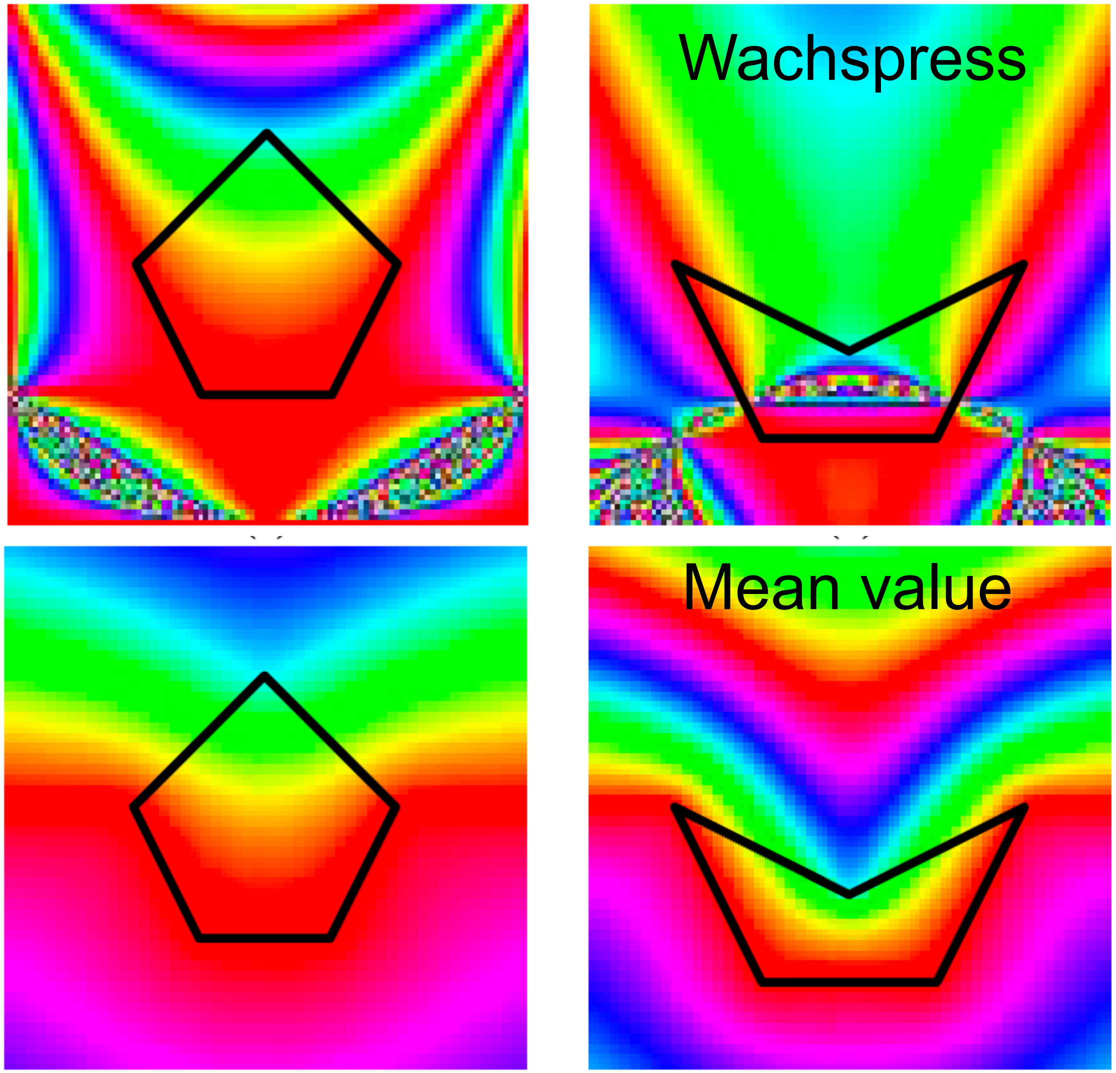

Mean Value Coordinates (MVC)

- Machinery

Circumferential Mean Value Theorem. *For a disc $B = B(v_0, r) \subset \Omega$ with boundary Γ,*

$$u(v_0) = \frac{1}{2\pi r} \int_{\Gamma} u(v)\,\mathrm{d}s.$$

$$u_{\mathcal{T}}(v_0) = \frac{1}{2\pi r} \sum_{i=1}^{k} \int_{\Gamma_i} u_{\mathcal{T}}(v)\,ds,$$

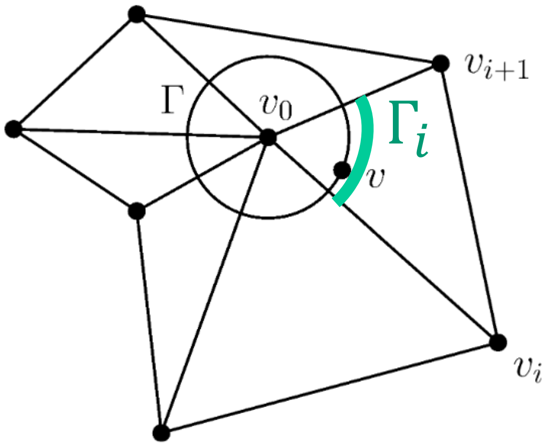

Fig. 2. Circle for the Mean Value Theorem.

- Piecewise linear discretization

Lemma 1. *If $f : T_i \to \mathbb{R}$ is any linear function then*

$$\int_{\Gamma_i} f(v)\,\mathrm{d}s = r\alpha_i f(v_0) + r^2 \tan(\alpha_i/2)\left(\frac{f(v_i) - f(v_0)}{\|v_i - v_0\|} + \frac{f(v_{i+1}) - f(v_0)}{\|v_{i+1} - v_0\|}\right).$$

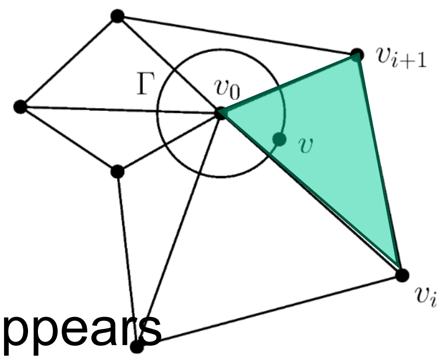

- Substituting lemma 1 into $u_{\mathcal{T}}(v_0) = \frac{1}{2\pi r} \sum_{i=1}^{k} \int_{\Gamma_i} u_{\mathcal{T}}(v)\,ds,$ and r disappears

$$\boxed{0 = \sum_{i=1}^{k} \tan(\alpha_i/2) \left(\frac{u_{\mathcal{T}}(v_i) - u_{\mathcal{T}}(v_0)}{||v_i - v_0||} + \frac{u_{\mathcal{T}}(v_{i+1}) - u_{\mathcal{T}}(v_0)}{||v_{i+1} - v_0||} \right)}$$

Follow-ups of MVC

- **MVC for 3D triangular cages [Ju et al. 2005]**
  - Still has closed-form expressions

// Robust evaluation on a triangular mesh
for each vertex p_j with values f_j
    $d_j \leftarrow \|p_j - x\|$
    if $d_j < \varepsilon$ return f_j
    $u_j \leftarrow (p_j - x)/d_j$
$totalF \leftarrow 0$
$totalW \leftarrow 0$
for each triangle with vertices p_1, p_2, p_3 and values f_1, f_2, f_3
    $l_i \leftarrow \|u_{i+1} - u_{i-1}\|$ *// for* $i = 1,2,3$
    $\theta_i \leftarrow 2\arcsin[l_i/2]$
    $h \leftarrow (\sum \theta_i)/2$
    if $\pi - h < \varepsilon$
        // x lies on t, use 2D barycentric coordinates
        $w_i \leftarrow \sin[\theta_i] l_{i-1} l_{i+1}$
        return $(\sum w_i f_i)/(\sum w_i)$
    $c_i \leftarrow (2\sin[h]\sin[h - \theta_i])/(\sin[\theta_{i+1}]\sin[\theta_{i-1}]) - 1$
    $s_i \leftarrow \mathrm{sign}[det[u_1, u_2, u_3]]\sqrt{1 - c_i^2}$
    if $\exists i, |s_i| \leq \varepsilon$
        // x lies outside t on the same plane, ignore t
        continue
    $w_i \leftarrow (\theta_i - c_{i+1}\theta_{i-1} - c_{i-1}\theta_{i+1})/(d_i \sin[\theta_{i+1}] s_{i-1})$
    $totalF += \sum w_i f_i$
    $totalW += \sum w_i$
$f_x \leftarrow totalF / totalW$

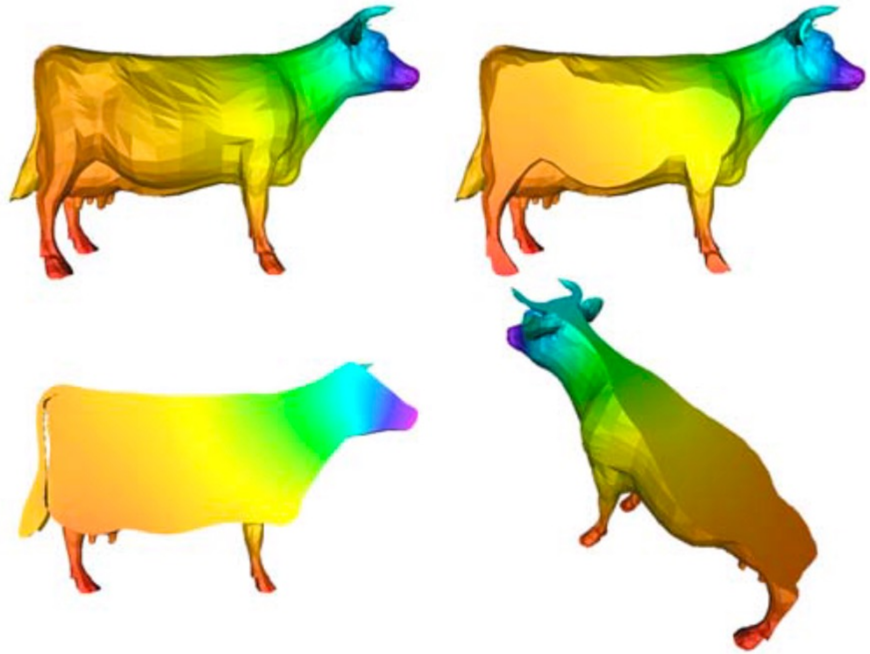

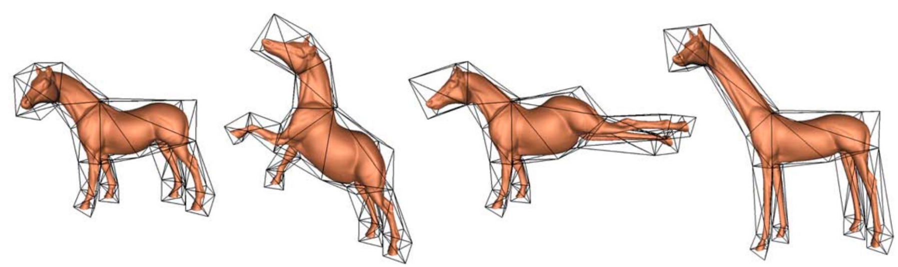

(a) (b) (c) (d)

Follow-ups of MVC

- **Positive MVC [Lipman et al. 2007]**
  - Computing MVC based on the visible part of the cage from the query point
  - No closed-form expressions, computed numerically
  - Relying on GPU implementation to stay comparable efficiency as MVC

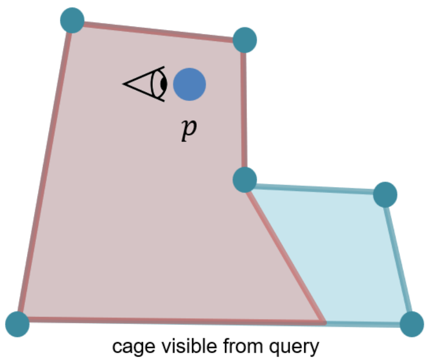

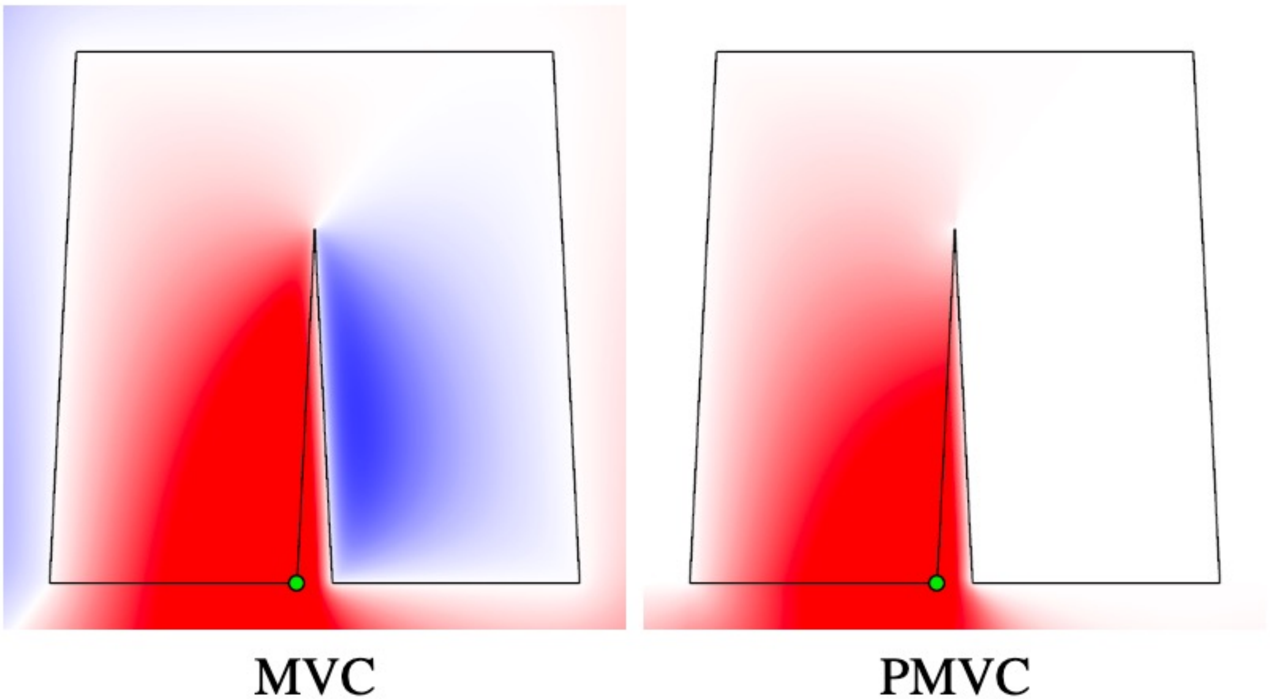

Follow-ups of MVC

- **Positive MVC [Lipman et al. 2007]**
  - Computing MVC based on the visible part of the cage from the query point
  - No closed-form expressions, computed numerically
  - Relying on GPU implementation to stay comparable efficiency as MVC

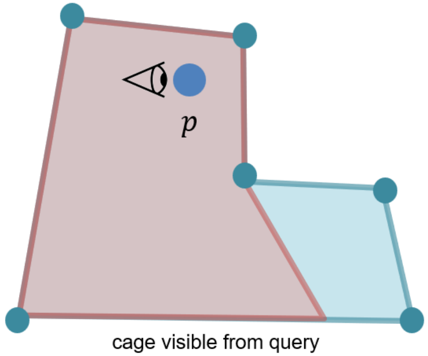

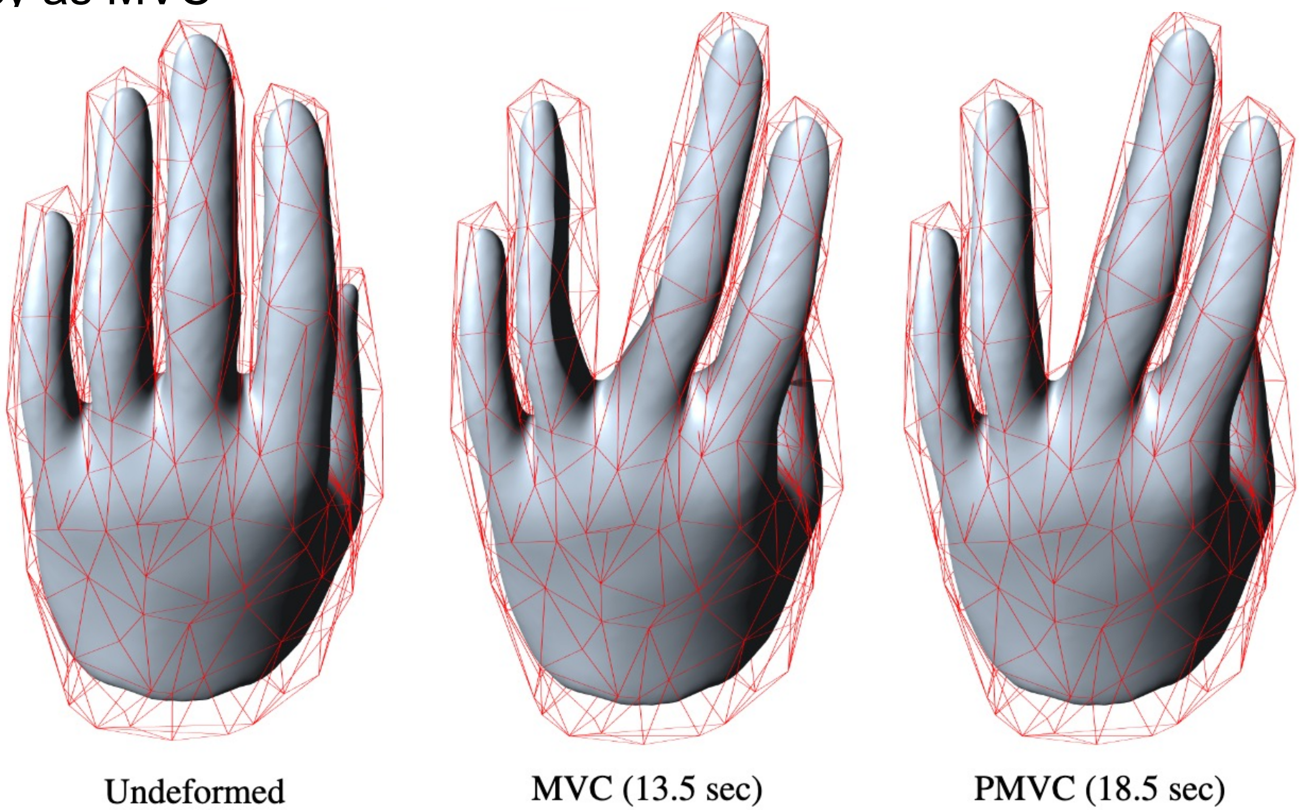

Follow-ups of MVC

- Non-triangular cages need to be triangulated
- Cage triangulation can cause artifacts
  - Symmmetry breaking

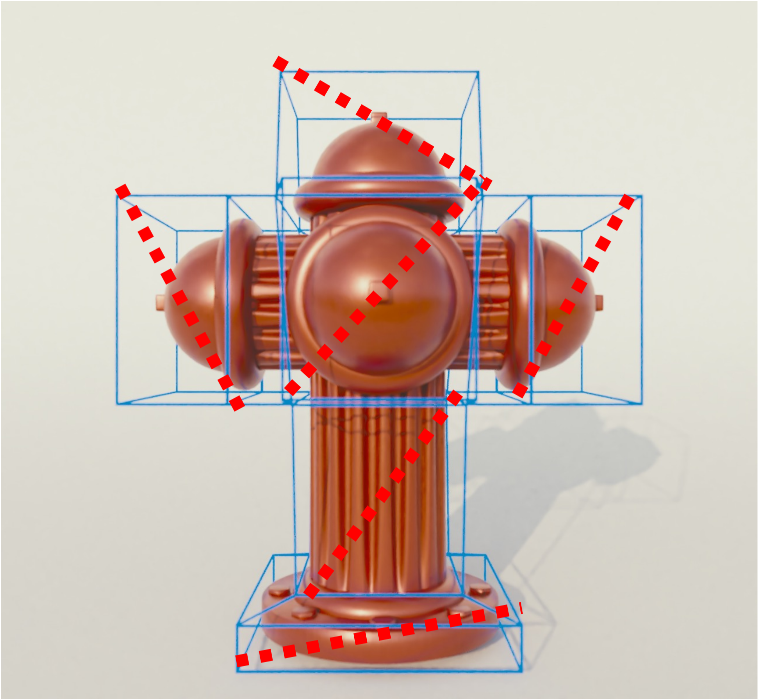

undeformed

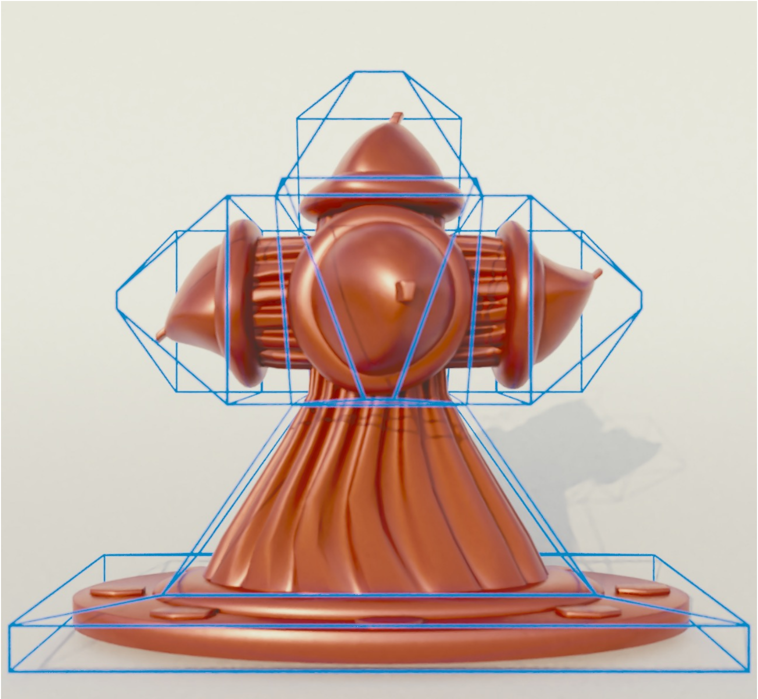

MVC

Follow-ups of MVC

- **QMVC** [Thiery et al. 2018]
  - Closed-form expressions for quad cages
  - No artifacts due to cage triangulation
  - Intuitive moldeing

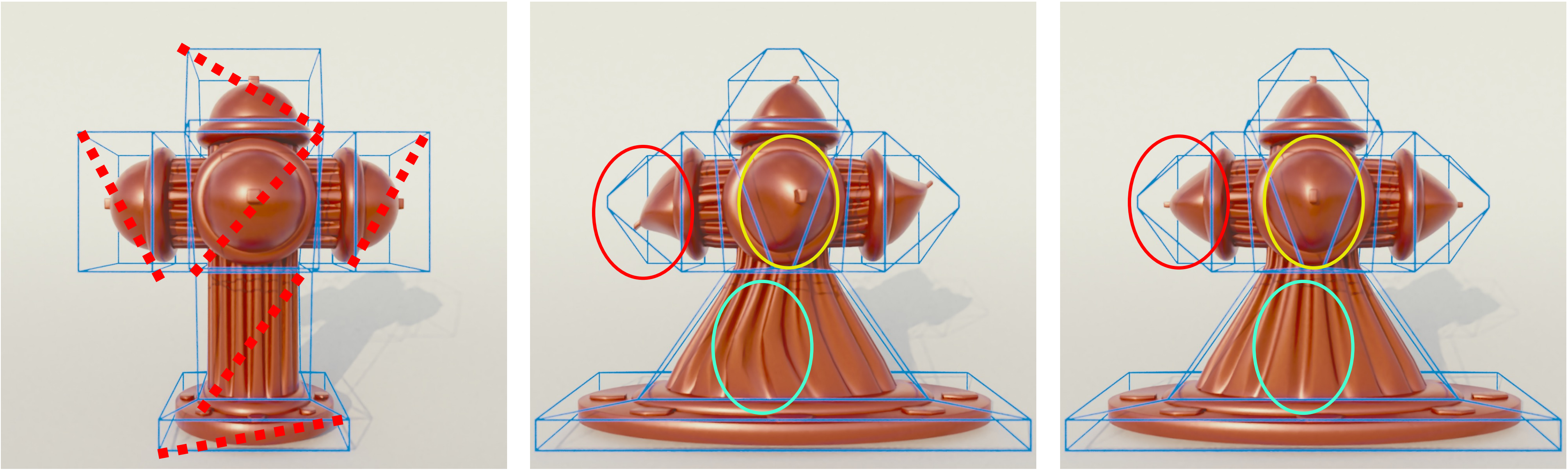

undeformed **MVC** **QMVC**

Follow-ups of MVC

- **Cublic MVC [Li et al. 2013]**
  - First work on curved boundary instead of piecewise linear boundary
  - Fewer control points for smooth deformation
  - Of course computing integral is more complicated

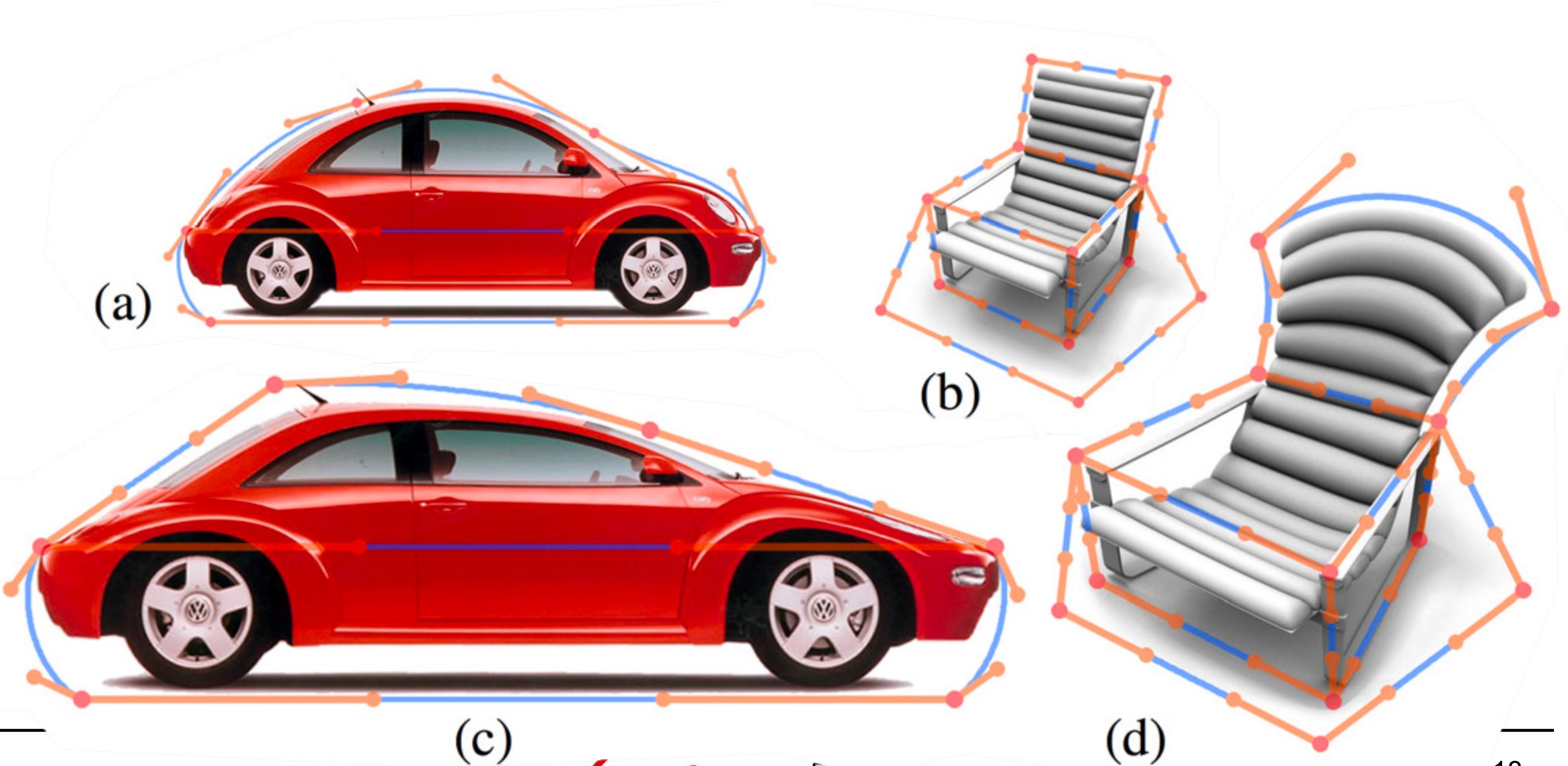

Follow-ups of MVC

- **Stochastic computations of GBC** [de Goes et al. 2024]
  - Formulating GBC as kernel-based least-squares minimization

$$\widehat{\alpha}_v(\mathrm{x}) = \Lambda_v(\mathrm{x}, \mathrm{x}) = \mathbf{u}_v(\mathrm{x})^t \mathbf{x}.$$

Follow-ups of MVC

- **Stochastic computations of GBC** [de Goes et al. 2024]
  - Formulating GBC as kernel-based least-squares minimization

$$\widehat{\alpha}_v(\mathrm{x}) = \Lambda_v(\mathrm{x}, \mathrm{x}) = \boxed{\mathbf{u}_v(\mathrm{x})^t}\mathbf{x}.$$

$$\boxed{\mathbf{u}_v(\mathrm{x}) = \arg\min_{\mathbf{u}} \int_C \kappa(\mathrm{x}, \mathrm{y})\, \|\mathbf{u}^t\mathbf{y} - \phi_v(\mathrm{y})\|^2 dy.}$$

Follow-ups of MVC

- **Stochastic computations of GBC [de Goes et al. 2024]**
  - Formulating GBC as kernel-based least-squares minimization

$$\widehat{\alpha}_v(\mathrm{x}) = \Lambda_v(\mathrm{x},\mathrm{x}) = \boxed{\mathbf{u}_v(\mathrm{x})^t}\mathbf{x}.$$

$$\boxed{\mathbf{u}_v(\mathrm{x}) = \arg\min_{\mathbf{u}} \int_C \kappa(\mathrm{x},\mathrm{y}) \|\mathbf{u}^t\mathbf{y} - \phi_v(\mathrm{y})\|^2 dy.}$$

  - Monte-Carlo sampling for computing the integral over the cage surface

$$\mathbf{u}_v(\mathrm{x}) = \arg\min_{\mathbf{u}} \sum_k w_k \|\mathbf{u}^t\mathbf{y}_k - \phi_v(\mathrm{y}_k)\|^2.$$

$$\hat{\alpha}(x) = \boldsymbol{x}^t(\Sigma_k w_k \boldsymbol{y}_k \boldsymbol{y}_k^t)^{-1}(\Sigma_k \phi_v(y_k)\boldsymbol{y}_k)$$

A small 4x4 linear solve for each query point

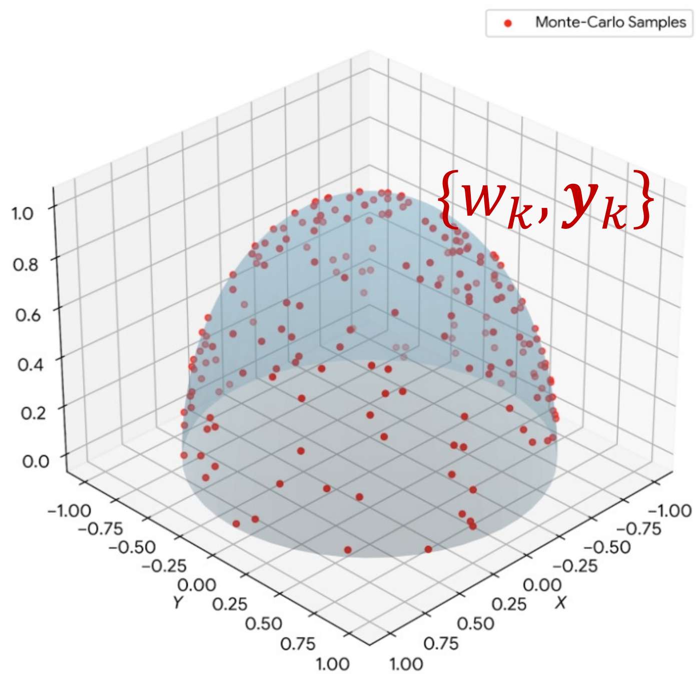

Follow-ups of MVC

- **Stochastic computations of GBC** **[de Goes et al. 2024]**
  - Formulating GBC as kernel-based least-squares minimization

$$\widehat{\alpha}_v(\mathrm{x}) = \Lambda_v(\mathrm{x},\mathrm{x}) = \boxed{\mathbf{u}_v(\mathrm{x})^t}\,\mathbf{x}. \qquad \boxed{\mathbf{u}_v(\mathrm{x}) = \arg\min_{\mathbf{u}} \int_C \kappa(\mathrm{x},\mathrm{y})\,\|\mathbf{u}^t\mathbf{y} - \phi_v(\mathrm{y})\|^2 dy.}$$

  - Monte-Carlo sampling for computing the integral over the cage surface

$$\mathbf{u}_v(\mathrm{x}) = \arg\min_{\mathbf{u}} \sum_k w_k \|\mathbf{u}^t\mathbf{y}_k - \phi_v(\mathrm{y}_k)\|^2. \qquad \hat{\alpha}(x) = \boldsymbol{x}^t\left(\Sigma_k w_k \boldsymbol{y}_k \boldsymbol{y}_k^t\right)^{-1}\left(\Sigma_k \phi_v(y_k)\boldsymbol{y}_k\right)$$

A small 4x4 linear solve for each query point

  - Agnostic to cage discretization!

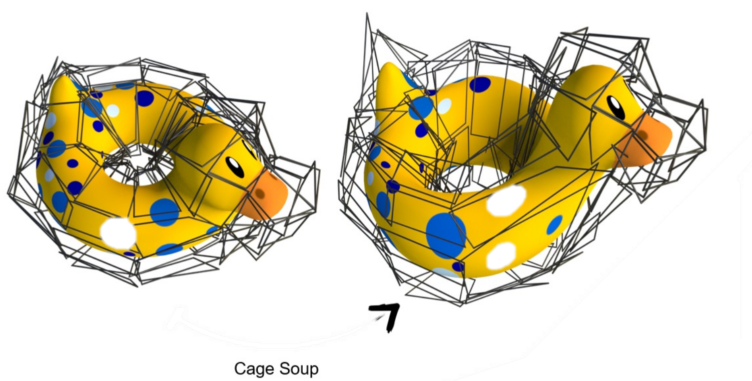

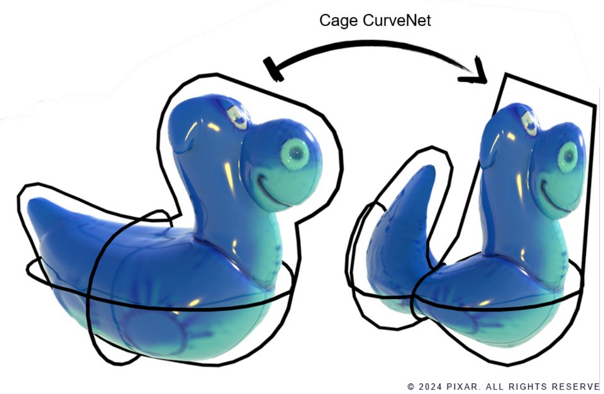

Follow-ups of MVC

- **Stochastic computations of GBC [de Goes et al. 2024]**
  - Formulating GBC as kernel-based least-squares minimization

$$\widehat{\alpha}_v(\mathrm{x}) = \Lambda_v(\mathrm{x},\mathrm{x}) = \boxed{\mathbf{u}_v(\mathrm{x})^t}\,\mathbf{x}. \qquad \boxed{\mathbf{u}_v(\mathrm{x}) = \arg\min_{\mathbf{u}} \int_C \kappa(\mathrm{x},\mathrm{y})\,\|\mathbf{u}^t\mathbf{y} - \phi_v(\mathrm{y})\|^2 dy.}$$

  - Monte-Carlo sampling for computing the integral over the cage surface

$$\mathbf{u}_v(\mathrm{x}) = \arg\min_{\mathbf{u}} \sum_k w_k \|\mathbf{u}^t\mathbf{y}_k - \phi_v(\mathrm{y}_k)\|^2. \qquad \hat{\alpha}(x) = \boldsymbol{x}^t\left(\Sigma_k w_k \boldsymbol{y}_k \boldsymbol{y}_k^t\right)^{-1}\left(\Sigma_k \phi_v(y_k)\boldsymbol{y}_k\right)$$

A small 4x4 linear solve for each query point

  - Agnostic to cage discretization!

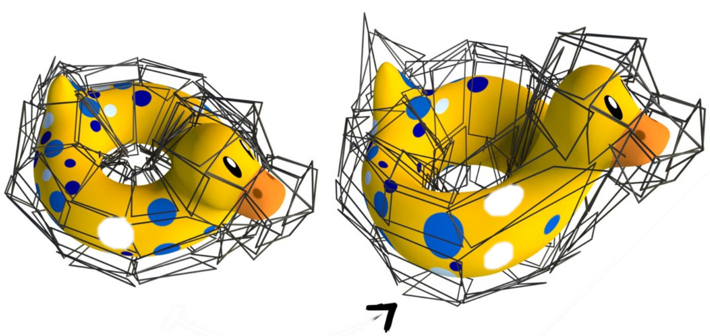

Cage Soup

Cage CurveNet

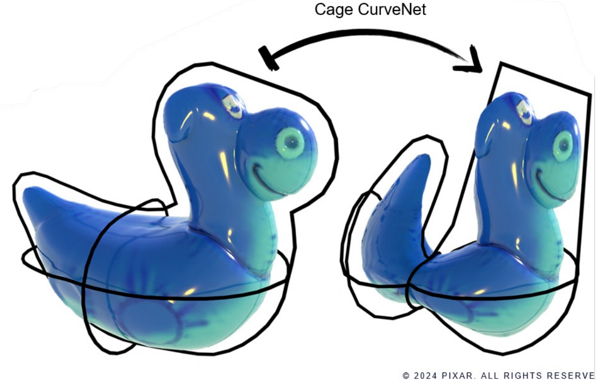

  - Reproducing MVC, PMVC, HC by different strategies to sample $\{w_k, \boldsymbol{y}_k\}$

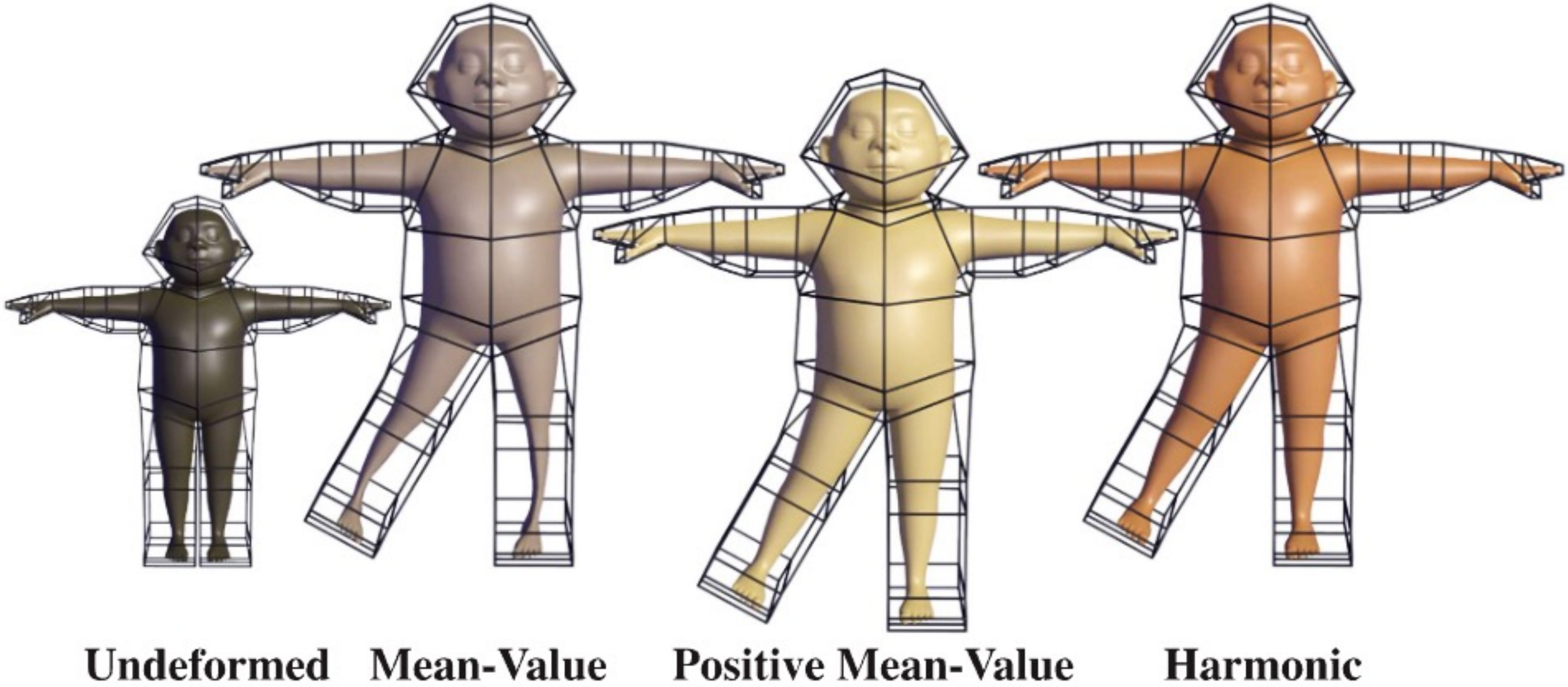

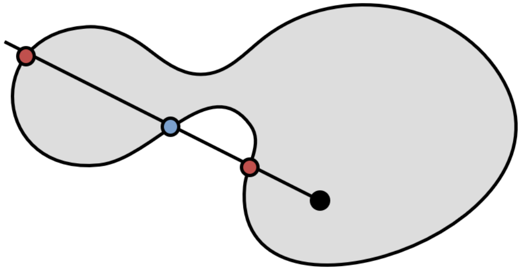

Ray tracing $\{(y_k, (-1)^k/d_k)\}$

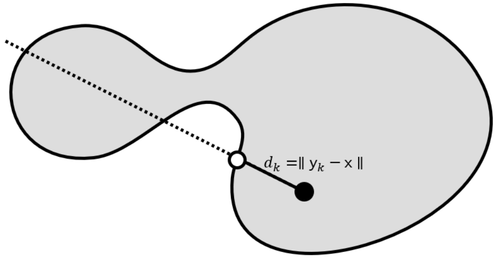

Ray tracing $\{(y_k, 1/d_k)\}$

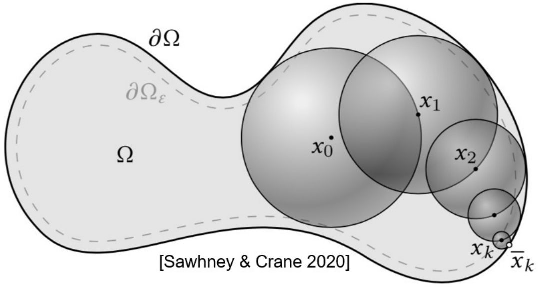

Walk on Spheres $\{(y_k, 1)\}$

Key remarks on closed-form MVC

- Advantages
  - Works for concave shapes
  - Fast pointwise evaluation through closed-form expressions, in most of the cases
  - Smoothness
- Disadvantages
  - Artifacts due to potential negative values
  - Enforcing non-negativeness requires extra computational cost

GBC without closed-form expressions

Harmonic Coordinates [Joshi et al. 2007]

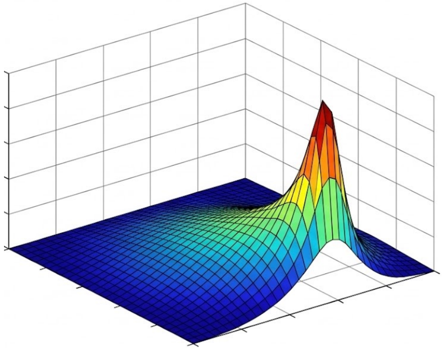

- Machinery
  - Solve Laplace's equation to obtain GBC
    - Inside cage: $\Delta\lambda_i(x) = 0, x \in \text{Int}C$
    - Lagrange property: $\lambda_i(c_j) = \delta_{i,j}, x \in C$
- Discretization
  - Tessellating the entire volume including the cage surface
- Solve the coordinates numerically
  - Large sparse linear systems
  - Solving N_C times for all $\{\lambda_i(x)\}$

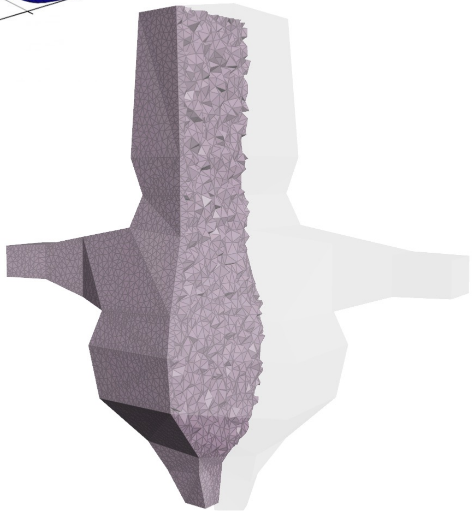

Advantages:
+ Positive
+ Locality

Disadvantages:
— Costly
— C^0 smoothness
— No pointwise evaluation

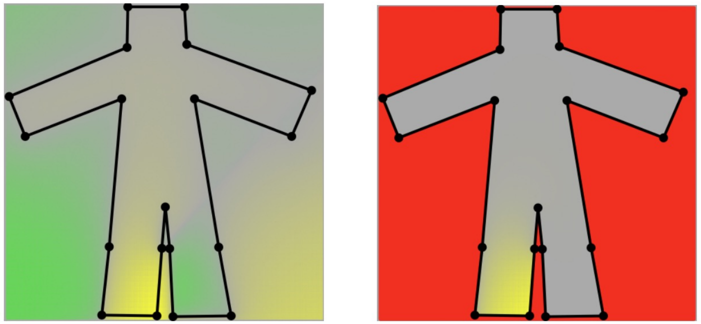

MVC HC

Maximum Entropy Coordinates [Hormann et al. 2008]

- Machinery
  - Maximum entropy principle
  - Needs an input prior function

$$\max_{b(v)\in\mathbb{R}^n_+} H(b,m), \qquad H(b,m) = -\sum_{i=1}^{n} b_i(v) \ln\left(\frac{b_i(v)}{m_i(v)}\right)$$

$$\sum_{i=1}^{n} b_i(v) = 1,$$
$$\sum_{i=1}^{n} b_i(v)(v_i - v) = 0$$

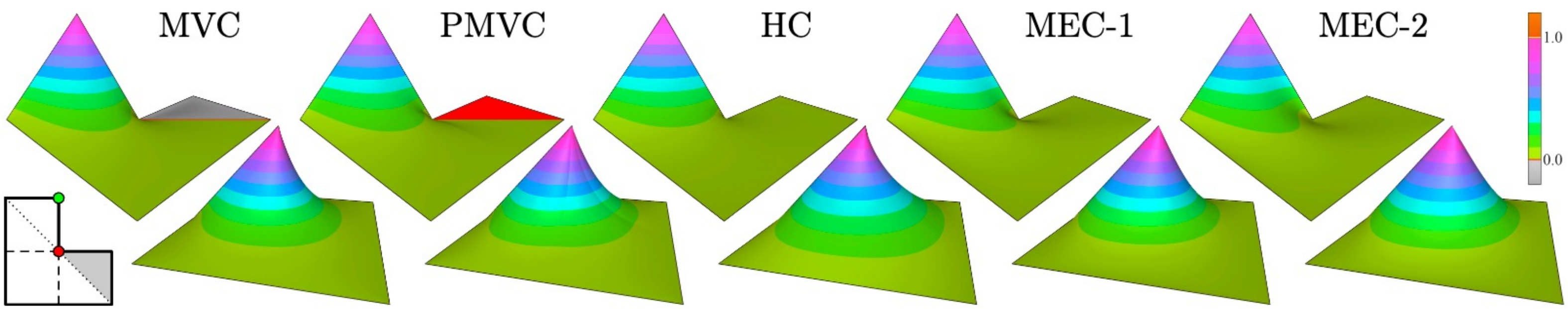

- Discretization
  - Only a point set is needed for encoding $m_i(v)$
- Numerical solve
  - Nonlinear convex optimization per query point solving for a 3D vector

Advantages:
+ Positive
+ Pointwise minimization
+ Supports arbitrary polygons

Disadvantages:
– Costly
– Bad choice of priors imposes artifacts

Maximum Entropy Coordinates [Hormann et al. 2008]

Edwin Thompson Jaynes

Interpretating statistical mechanics as a statistical inference problem

PHYSICAL REVIEW, Vol.
Printed in U. S.

Information Theory and Statistical Mechanics

E. T. JAYNES
Department of Physics, Stanford University, Stanford, California

(Received September 4, 1956; revised manuscript received March 4, 1957)

Information theory provides a constructive criterion for setting up probability distributions on the basis of partial knowledge, and leads to a type of statistical inference which is called the maximum-entropy estimate. It is the least biased estimate possible on the given information; i.e., it is maximally noncommittal with regard to missing information. If one considers statistical mechanics as a form of statistical inference rather than as a physical theory, it is found that the usual computational rules, starting with the determination of the partition function, are an immediate consequence of the maximum-entropy principle. In the resulting "subjective statistical mechanics," the usual rules are thus justified independently of any physical argument, and in particular independently of experimental verification; whether or not the results agree with experiment, they still represent the best estimates that could have been made on the basis of the information available.

It is concluded that statistical mechanics need not be regarded as a physical theory dependent for its validity on the truth of additional assumptions not contained in the laws of mechanics (such as ergodicity, metric transitivity, equal *a priori* probabilities, etc.). Furthermore, it is possible to maintain a sharp distinction between its physical and statistical aspects. The former consists only of the correct enumeration of the states of a system and their properties; the latter is a straightforward example of statistical inference.

1. INTRODUCTION

THE recent appearance of a very comprehensive survey[1] of past attempts to justify the methods of statistical mechanics in terms of mechanics, classical or quantum, has helped greatly, and at a very opportune time, to emphasize the unsolved problems in this field.

Although the subject has been under development for many years, we still do not have a complete and satisfactory theory, in the sense that there is no line of argument proceeding from the laws of microscopic mechanics to macroscopic phenomena, that is generally regarded by physicists as convincing in all respects. Such an argument should (a) be free from objection on mathematical grounds, (b) involve no additional arbi-

[1] D. ter Haar, Revs. Modern Phys. 27, 289 (1955).

way, and obtains the result

$$p_i = e^{-\lambda-\mu f(x_i)}. \qquad (2\text{-}4)$$

The constants λ, μ are determined by substituting into (2-1) and (2-2). The result may be written in the form

$$\langle f(x)\rangle = -\frac{\partial}{\partial\mu}\ln Z(\mu), \qquad (2\text{-}5)$$

$$\lambda = \ln Z(\mu), \qquad (2\text{-}6)$$

where

$$Z(\mu)=\textstyle\sum_i e^{-\mu f(x_i)} \qquad (2\text{-}7)$$

will be called the partition function.

This may be generalized to any number of functions $f(x)$: given the averages

$$\langle f_r(x)\rangle = \textstyle\sum_i p_i f_r(x_i), \qquad (2\text{-}8)$$

form the partition function

$$Z(\lambda_1,\cdots,\lambda_m) = \textstyle\sum_i \exp\{-[\lambda_1 f_1(x_i)+\cdots+\lambda_m f_m(x_i)]\}. \qquad (2\text{-}9)$$

Then the maximum-entropy probability distribution is given by

$$p_i = \exp\{-[\lambda_0+\lambda_1 f_1(x_i)+\cdots+\lambda_m f_m(x_i)]\}, \qquad (2\text{-}10)$$

in which the constants are determined from

$$\langle f_r(x)\rangle = -\frac{\partial}{\partial\lambda_r}\ln Z, \qquad (2\text{-}11)$$

$$\lambda_0 = \ln Z. \qquad (2\text{-}12)$$

The entropy of the distribution (2-10) then reduces to

$$S_{\max} = \lambda_0+\lambda_1\langle f_1(x)\rangle+\cdots+\lambda_m\langle f_m(x)\rangle, \qquad (2\text{-}13)$$

where the constant K in (2-3) has been set equal to unity. The variance of the distribution of $f_r(x)$ is found to be

$$\Delta^2 f_r = \langle f_r^2\rangle - \langle f_r\rangle^2 = \frac{\partial^2}{\partial\lambda_r^2}(\ln Z). \qquad (2\text{-}14)$$

In addition to its dependence on x, the function f_r may contain other parameters $\alpha_1, \alpha_2, \cdots$, and it is easily shown that the maximum-entropy estimates of the derivatives are given by

$$\left\langle \frac{\partial f_r}{\partial \alpha_k}\right\rangle = -\frac{1}{\lambda_r}\frac{\partial}{\partial\alpha_k}\ln Z. \qquad (2\text{-}15)$$

The principle of maximum entropy may be regarded as an extension of the principle of insufficient reason (to which it reduces in case no information is given except enumeration of the possibilities x_i), with the following essential difference. The maximum-entropy distribution may be asserted for the positive reason that it is uniquely determined as the one which is maximally noncommittal with regard to missing information, instead of the negative one that there was no reason to think otherwise. Thus the concept of entropy supplies the missing criterion of choice which Laplace needed to remove the apparent arbitrariness of the principle of insufficient reason, and in addition it shows precisely how this principle is to be modified in case there are reasons for "thinking otherwise."

Mathematically, the maximum-entropy distribution has the important property that no possibility is ignored; it assigns positive weight to every situation that is not absolutely excluded by the given information. This is quite similar in effect to an ergodic property. In this connection it is interesting to note that prior to the work of Shannon other information measures had been proposed[12,13] and used in statistical inference, although in a different way than in the present paper. In particular, the quantity $-\sum p_i^2$ has many of the qualitative properties of Shannon's information measure, and in many cases leads to substantially the same results. However, it is much more difficult to apply in practice. Conditional maxima of $-\sum p_i^2$ cannot be found by a stationary property involving Lagrangian multipliers, because the distribution which makes this quantity stationary subject to prescribed averages does not in general satisfy the condition $p_i \geq 0$. A much more important reason for preferring the Shannon measure is that it is the only one which satisfies the condition of consistency represented by the composition law (Appendix A). Therefore one expects that deductions made from any other information measure, if carried far enough, will eventually lead to contradictions.

3. APPLICATION TO STATISTICAL MECHANICS

It will be apparent from the equations in the preceding section that the theory of maximum-entropy inference is identical in mathematical form with the rules of calculation provided by statistical mechanics. Specifically, let the energy levels of a system be

$$E_i(\alpha_1,\alpha_2,\cdots),$$

where the external parameters α_i may include the volume, strain tensor applied electric or magnetic fields, gravitational potential, etc. Then if we know only the average energy $\langle E\rangle$, the maximum-entropy probabilities of the levels E_i are given by a special case of (2-10), which we recognize as the Boltzmann distribution. This observation really completes our derivation

[12] R. A. Fisher, Proc. Cambridge Phil. Soc. 22, 700 (1925).
[13] J. L. Doob, Trans. Am. Math. Soc. 39, 410 (1936).

Local Barycentric Coordinates [Zhang et al. 2014]

- Machinery
  - minimize total variation (TV) of GBC

$$\min_{w_1,\ldots,w_n} \sum_{i=1}^{n} \int_\Omega |\nabla w_i|$$

$$\text{s.t.} \sum_{i=1}^{n} w_i(\mathbf{x})\mathbf{c}_i = \mathbf{x}, \ \sum_{i=1}^{n} w_i = 1, \ w_i \geq 0, \ \forall \mathbf{x} \in \Omega,$$

$$w_i(\mathbf{c}_j) = \delta_{ij} \ \forall i, j,$$

w_i is linear on cage edges and faces $\forall i$.

$$\sum_{i=1}^{n} \int_\Omega \phi_i |\nabla w_i|,$$

Advantages:
+ Control over locality

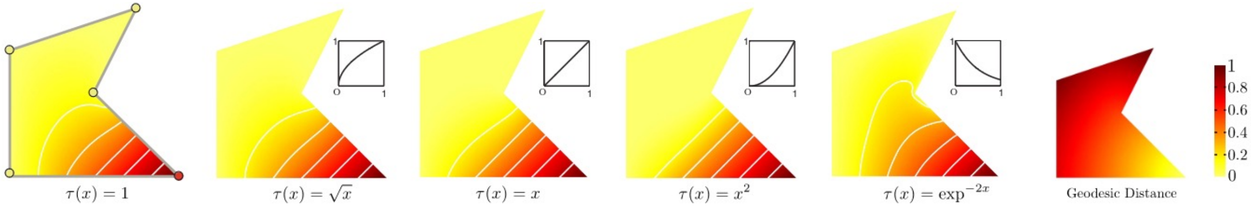

[ZDL*14]

Disadvantages:
— Guarantees only C^1-continuity
— Complex computation

Variational Barycentric Coordinates [Dodik et al. 2023]

- Continuous formulation

$$\min_{\alpha_{i\in[1,K]}} \sum_{i=1}^{K} \int_{\mathcal{P}} F[\alpha_i(x), \nabla\alpha_i(x), \Delta\alpha_i(x)]\,\mathrm{d}V(x), \quad (3)$$

$$\text{s.t.} \quad \alpha_i(x) \geq 0\,,\ \forall \alpha_i, x, \quad \text{(non-negativity)} \quad (3.1)$$

$$\textstyle\sum_i \alpha_i(x) = 1\,,\ \forall x, \quad \text{(partition of unity)} \quad (3.2)$$

$$\alpha_i(v_j) = \delta_{ij}\,,\ \forall \alpha_i, v_j \quad \text{(Lagrange property)} \quad (3.3)$$

$$\textstyle\sum_i \alpha_i(x) v_i = x\,,\ \forall x, \quad \text{(reproduction)} \quad (3.4)$$

- Representation
  - Neural network for $\alpha_i(x)$
- Solving for the coordinates
  - Adam optimizer

	Star	Gecko	Woody	Elephant	Blue Monster	Horse	Bust of Sappho	Hand	Armadillo
Cage vertices	12	34	26	64	100	51	40	92	110
Possible simplices	220	5984	2600	41664	16170	249900	91390	2794155	5773185
Interior simplices	68	388	738	1923	5255	3247	83958	35462	56438
Used simplices	68	388	403	803	1469	1072	1308	3432	4153
Training time (min)	1.03	1.36	1.37	1.99	3.09	11.88	15.45	35.32	43.05
Inference time (ms)	3.64	4.49	4.66	7.17	11.41	42.70	56.78	136.26	169.66

Weighted total variation

$$\mathrm{TV}(\boldsymbol{\alpha}) = \sum_{i=1}^{K} \int_{\mathcal{P}} \Psi(d(\boldsymbol{x}, \boldsymbol{v}_i))\,\|\nabla\alpha_i\|_2\,\mathrm{d}\boldsymbol{x},$$

Dirichlet energy

$$\mathrm{Dir}(\alpha_i) := \sum_{j=1}^{N} \int_{\mathcal{P}_j} \|\nabla\alpha_i\|_2^2\,\mathrm{d}\boldsymbol{x} + \sum_{j=1}^{M} \oint_{\partial\mathcal{P}_j} |\alpha_i^+ - \alpha_i^-|^2\,\mathrm{d}\boldsymbol{x}.$$

As-rigid-as-possible energy

$$\mathrm{ARAP}_{\boldsymbol{x}_i}(\varphi_{\boldsymbol{\alpha}}) \approx \sum_{j\in n(i)} \left\|(\varphi_{\boldsymbol{\alpha}}(\boldsymbol{x}_i) - \varphi_{\boldsymbol{\alpha}}(\boldsymbol{x}_j)) - R_i(\boldsymbol{x}_i - \boldsymbol{x}_j)\right\|_F^2,$$

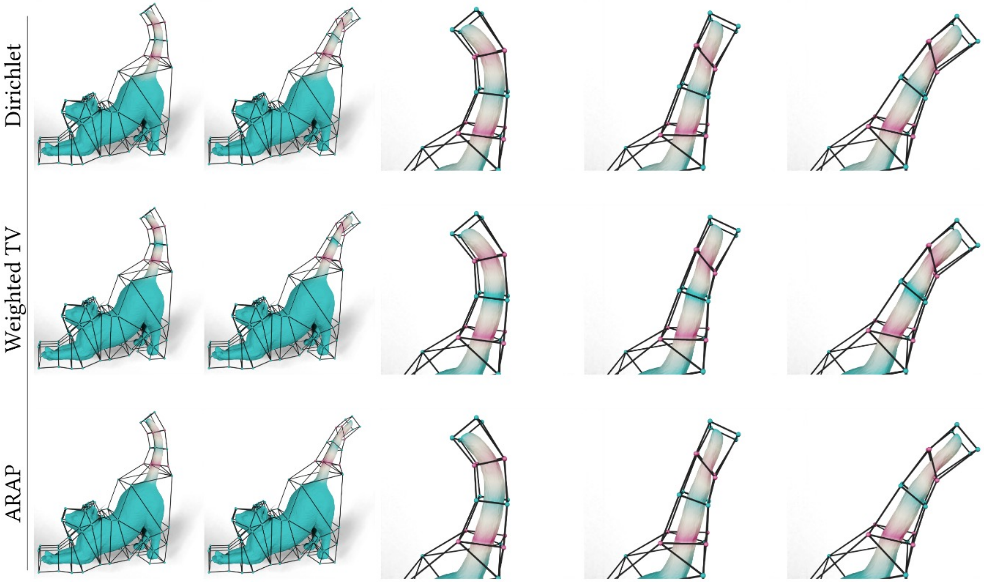

Remarks on minimization-based coordinates

- Advantages
  - They are positive
  - The resulting coordinates have better locality
  - High-quality due to their variational nature
- Disadvantages
  - Either relying on a mesh embedding the cage (discretize PDE)
  - Or, a neural network for representing the field
  - More costly to compute, via linear solvers or nonlinear optimizations

GBC with cage normals

Coordinates with normal control

- Add normal control to better preserve the model shape
  - Driven by the boundary reformulation of linear PDEs
- Advantages in efficiency
  - Pointwise evaluation often with closed-form expressions
  - No need to solve a linear system or nonlinear optimization
- Compromise in controllability
  - No longer interpolatory GBC
  - Deformation might get unintuitive

How to incorporate normal control?

- Instead of GBC λ_i for cage vertices
- Use ϕ_i for cage vertices and ψ_j for cage face normals

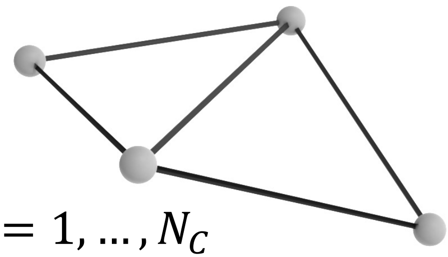

$\phi_i, i = 1, \ldots, N_C$

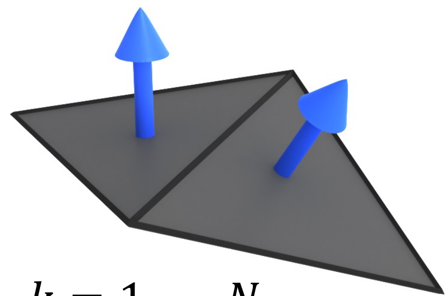

$\psi_k, k = 1, \ldots, N_F$

- Deformation control:

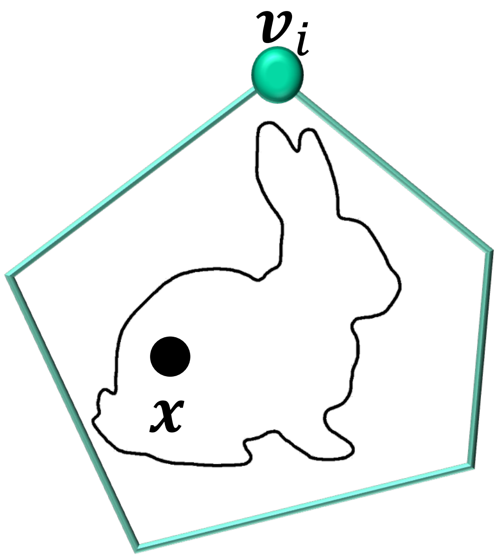

$$\boldsymbol{x} = \sum_i \phi_i(\boldsymbol{x})\boldsymbol{v}_i$$

$$\tilde{\boldsymbol{x}}(\boldsymbol{x}) = \sum_i \phi_i(\boldsymbol{x})\tilde{\boldsymbol{v}}_i$$

How to incorporate normal control?

- Instead of GBC λ_i for cage vertices
- Use ϕ_i for cage vertices and ψ_j for cage face normals

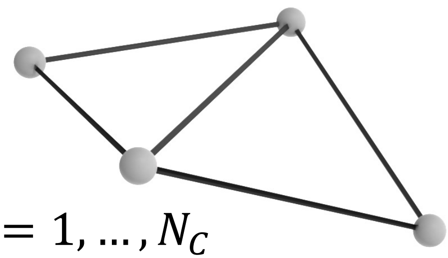

$\phi_i, i = 1, \dots, N_C$

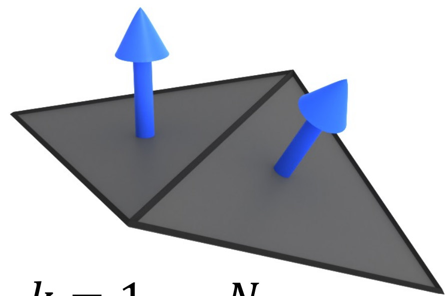

$\psi_k, k = 1, \dots, N_F$

- Deformation control:

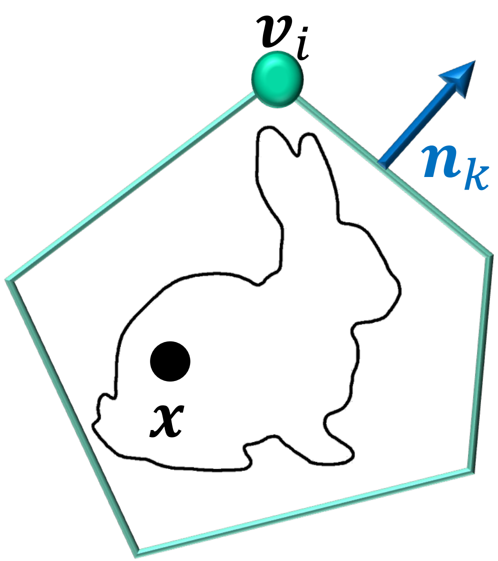

$$\boldsymbol{x} = \sum_i \phi_i(\boldsymbol{x})\boldsymbol{v}_i + \sum_k \psi_k(\boldsymbol{x})\boldsymbol{n}_k$$

$$\tilde{\boldsymbol{x}}(\boldsymbol{x}) = \sum_i \phi_i(\boldsymbol{x})\tilde{\boldsymbol{v}}_i + \sum_k \psi_k(\boldsymbol{x})\,(c_k\tilde{\boldsymbol{n}}_k)$$

Green Coordinates [Lipman et al. 2008]

- Machinery
  - Green's third identity for harmonic functions

$$G(x,y) = \frac{-1}{4\pi\|y-x\|}$$

$$u(y) = \int_{\partial\Omega} u\,(y)\,\frac{\partial G(y,x)}{\partial n_y}\,\mathrm{dA}_y - \int_{\partial\Omega} G\,(y,x)\,\frac{\partial u(y)}{\partial n_y}\,\mathrm{dA}_y$$

- Discretization
  - Triangular cages
    - Piecewise linear function for boundary values
    - Piecewise constant function for boundary flux

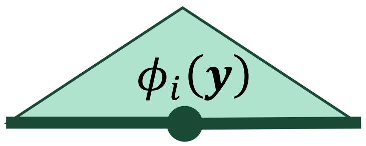

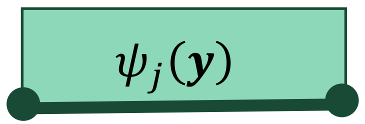

Green Coordinates [Lipman et al. 2008]

- Machinery
  - Green's third identity for harmonic functions

$$G(x,y) = \frac{-1}{4\pi\|y-x\|}$$

$$u(y) = \int_{\partial\Omega} u\,(y)\,\frac{\partial G(y,x)}{\partial n_y}\,\mathrm{dA}_y - \int_{\partial\Omega} G\,(y,x)\,\frac{\partial u(y)}{\partial n_y}\,\mathrm{dA}_y$$

- Discretization
  - Triangular cages
    - Piecewise linear function for boundary values
    - Piecewise constant function for boundary flux

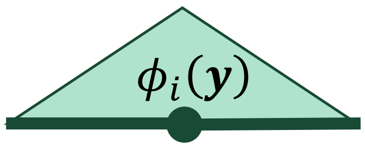

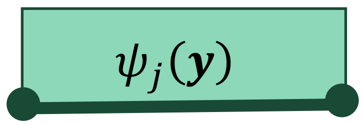

- Solver the coordinates
  - Closed-form expressions

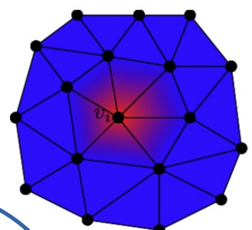

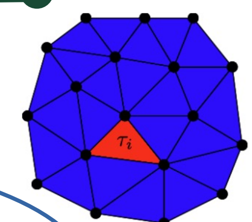

$$\phi_i(x) = \int_{\mathcal{N}\{v_i\}} \Gamma_i(y)\,\frac{\partial G(y,x)}{\partial n_y}\,\mathrm{dA}_y$$

$$\psi_j(x) = \int_{T_j} G(y,x)\,\mathrm{dA}_y$$

Closed-form Expressions of GC

Input: cage $P = (\mathbb{V}, \mathbb{T})$, set of points $\Lambda = \{\eta\}$
Output: $3D$ GC $\phi_i(\eta), \psi_j(\eta), i \in I_{\mathbb{V}}, j \in I_{\mathbb{T}}, \eta \in \Lambda$

```
/* Initialization                                  */
```
set all $\phi_i = 0$ and $\psi_j = 0$

```
/* Coordinate computation                          */
```
foreach *point* $\eta \in \Lambda$ **do**
  foreach *face* $j \in I_{\mathbb{T}}$ *with vertices* $v_{j_1}, v_{j_2}, v_{j_3}$ **do**
    foreach $\ell = 1,2,3$ **do**
      $v_{j_\ell} := v_{j_\ell} - \eta$
    $p := (v_{j_1} \cdot n(t_j))n(t_j)$
    foreach $\ell = 1,2,3$ **do**
      $s_\ell :=$
      $sign\left(((v_{j_\ell} - p) \times (v_{j_{\ell+1}} - p)) \cdot n(t_j)\right)$
      $I_\ell := \mathbf{GCTriInt}(p, v_{j_\ell}, v_{j_{\ell+1}}, 0)$
      $II_\ell := \mathbf{GCTriInt}(0, v_{j_{\ell+1}}, v_{j_\ell}, 0)$
      $q_\ell := v_{j_{\ell+1}} \times v_{j_\ell}$
      $N_\ell := q_\ell / \|q_\ell\|$
    $I := -\left|\sum_{k=1}^{3} s_k I_k\right|$
    $\psi_j(\eta) := -I$
    $w := n(t_j)I + \sum_{k=1}^{3} N_k II_k$
    if $\|w\| > \epsilon$ **then**
      foreach $\ell = 1,2,3$ **do**
        $\phi_{j_\ell}(\eta) := \phi_{j_\ell}(\eta) + \frac{N_{\ell+1} \cdot w}{N_{\ell+1} \cdot v_{j_\ell}}$
  end
end

[Lipman et al. 2008]

Procedure **GCTriInt**(p, v_1, v_2, η)
$\alpha := \cos^{-1}\left(\frac{(v_2 - v_1)\cdot(p - v_1)}{\|v_2 - v_1\|\|p - v_1\|}\right)$
$\beta := \cos^{-1}\left(\frac{(v_1 - p)\cdot(v_2 - p)}{\|v_1 - p\|\|v_2 - p\|}\right)$
$\lambda := \|p - v_1\|^2 \sin(\alpha)^2$
$c := \|p - \eta\|^2$
foreach $\theta = \pi - \alpha, \pi - \alpha - \beta$ **do**
  $S := \sin(\theta)$; $C := \cos(\theta)$
  $I_\theta := \frac{-sign(S)}{2}\left[2\sqrt{c}\tan^{-1}\left(\frac{\sqrt{c}C}{\sqrt{\lambda + S^2 c}}\right) + \right.$
  $\left.\sqrt{\lambda}\log\left(\frac{2\sqrt{\lambda}S^2}{(1-C)^2}\left(1 - \frac{2cC}{c(1+C)+\lambda+\sqrt{\lambda^2+\lambda c S^2}}\right)\right)\right]$
return $\frac{-1}{4\pi}\left|I_{\pi-\alpha} - I_{\pi-\alpha-\beta} - \sqrt{c}\beta\right|$

Algorithm 2: $3D$ Green Coordinates algorithm.

Appendix A [Ben-Chen et al. 2009]

The mappings φ and ψ. The mappings φ and ψ are defined on the vertices and faces of the mesh, respectively, so we must provide for each face a scalar value ψ_t and for each vertex a scalar value φ_v. The values of φ_v are determined as a sum of values on the faces neighboring v. Given a point $p \in \Omega$, and a face $t = (u,v,w) \in F$, we define a tetrahedron T spanned by these four points, as in Figure 15.

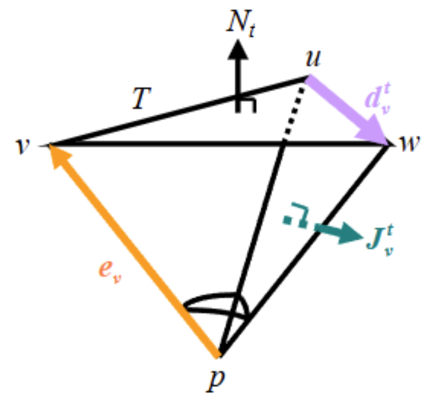

$$\tilde{e}_v = \frac{e_v}{\|e_v\|}$$
$$R_v^t = \|e_w\| + \|e_u\|$$
$$C_v^t = \frac{1}{4\pi\|d_v^t\|}\log\left(\frac{R_v^t + \|d_v^t\|}{R_v^t - \|d_v^t\|}\right)$$
$$\tilde{C}_v^t = \frac{1}{2\pi\left(R_v^t + \|d_v^t\|\right)\left(R_v^t - \|d_v^t\|\right)}$$
$$P_t = N_t \times \sum_{i \in t} d_i^t C_i^t - \omega_t N_t$$

Figure 15: *Notations for the definitions of $\varphi_v(p)$, $\psi_t(p)$ and their derivatives.*

On this tetrahedron, $4\pi\omega_t$ is the signed solid angle at the point p, subtended by the face t, and vol_t is its signed volume. N_t is the normalized outward pointing normal of t, and A_t is the area of the face t. Following Urago [2000] we obtain:

$$\psi_t = -\sum_{i \in t} C_i^t\left(J_i^t \cdot N_t\right) - \frac{3}{A_t}\omega_t vol_t$$

$$\varphi_v = \sum_{t \in N(v)} \frac{1}{2A_t} P_t \cdot J_v^t$$

Green Coordinates [Lipman et al. 2008]

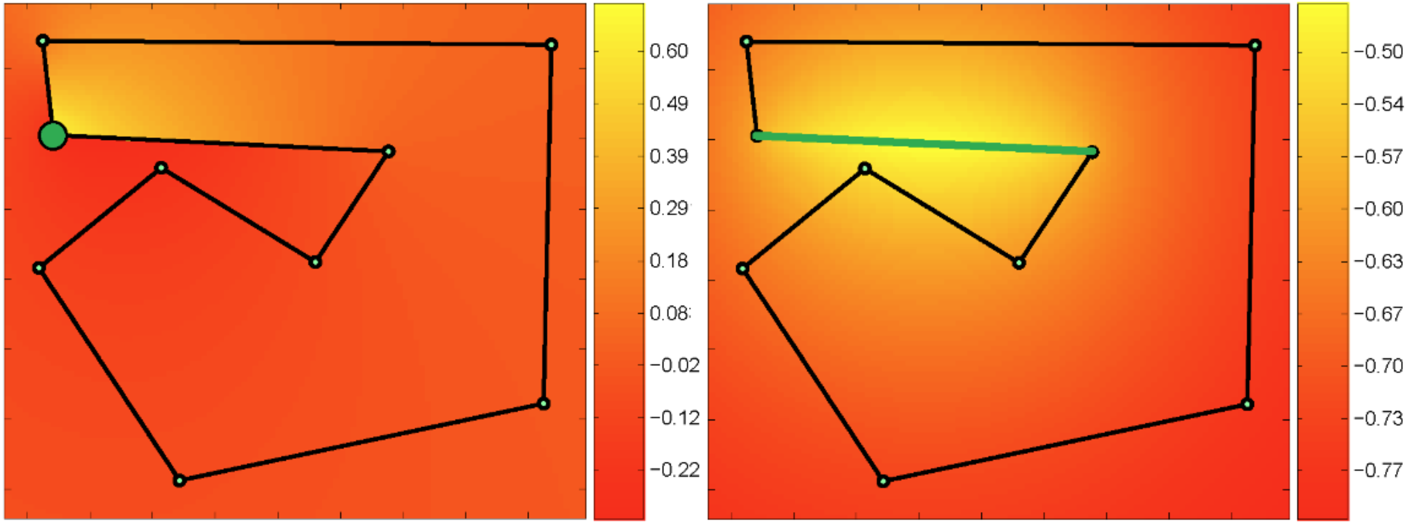

- Mathematical properties
  - Linear reproduction
  - Translational invariance
  - Rotation and scale invariance
  - C^{∞}-smoothness
  - Conformal mapping in 2D
  - Quasi-conformal in 3D

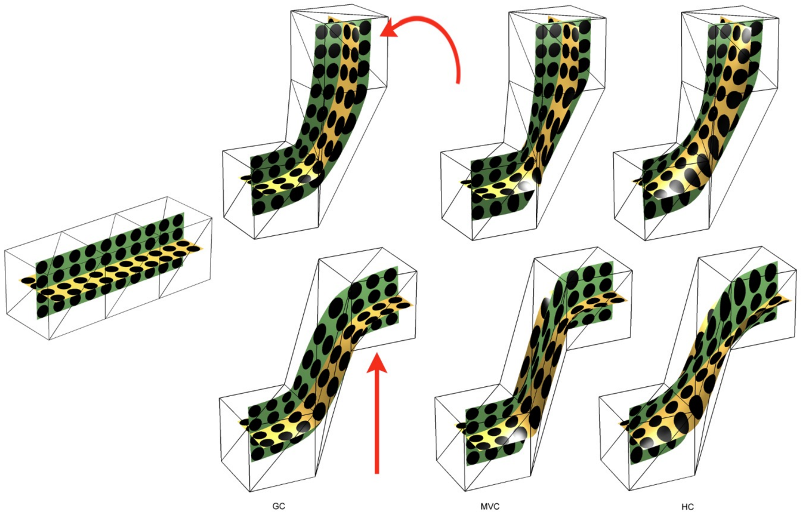

Properties of GC

- Advantages
  - Conformality mostly leads to better shape preservation
  - Allow for extrapolation outside of the cage
  - Easy to compute
- Disadvantages
  - Only for triangular cages
  - Not interpolatory

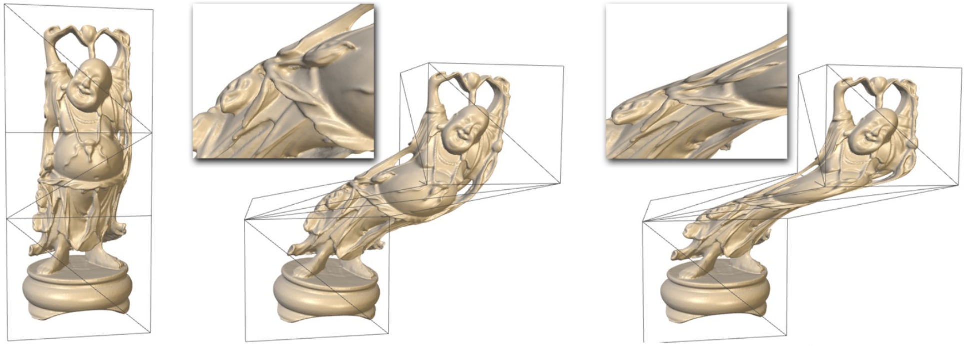

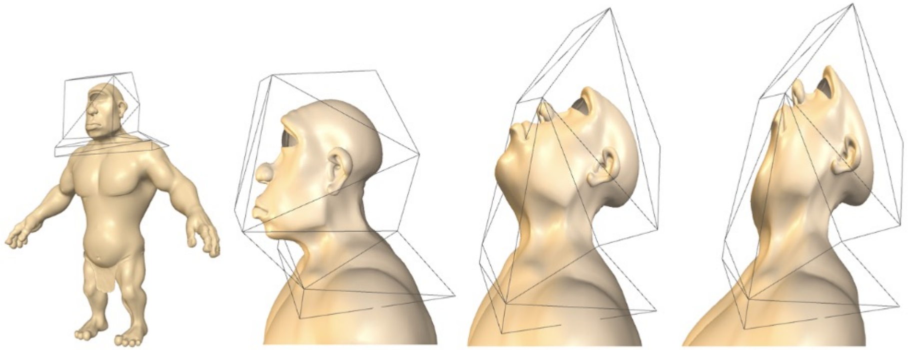

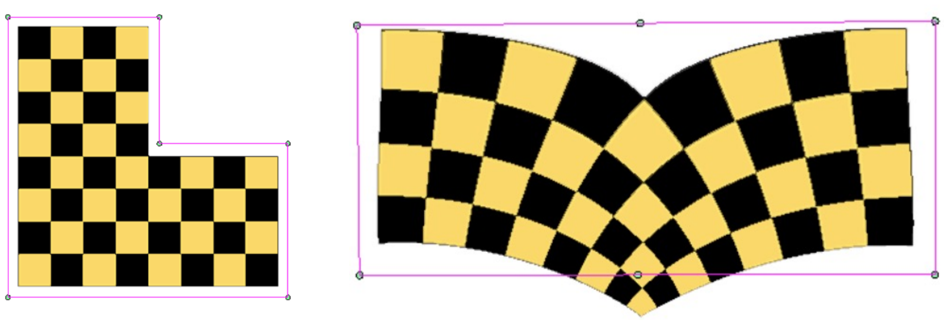

Follow-ups of GC

- Quad-based GC [Thiery et al. 2022]

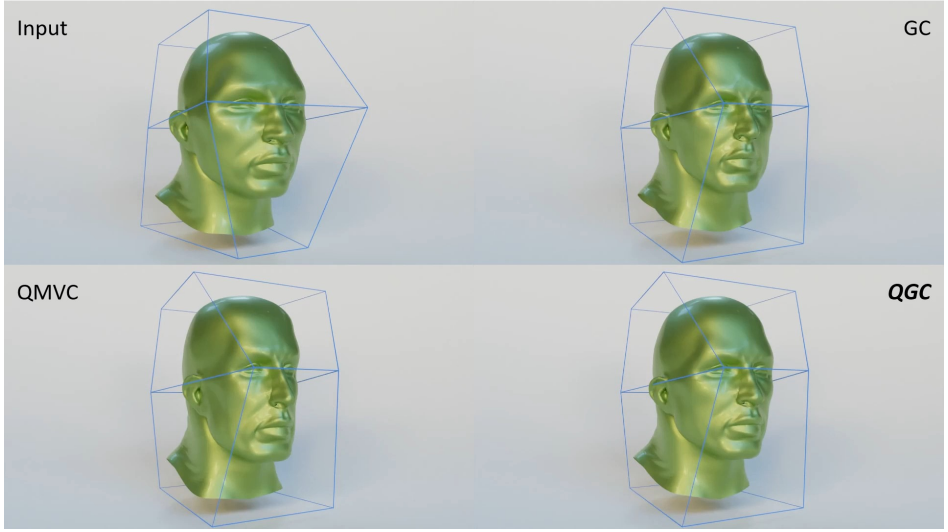

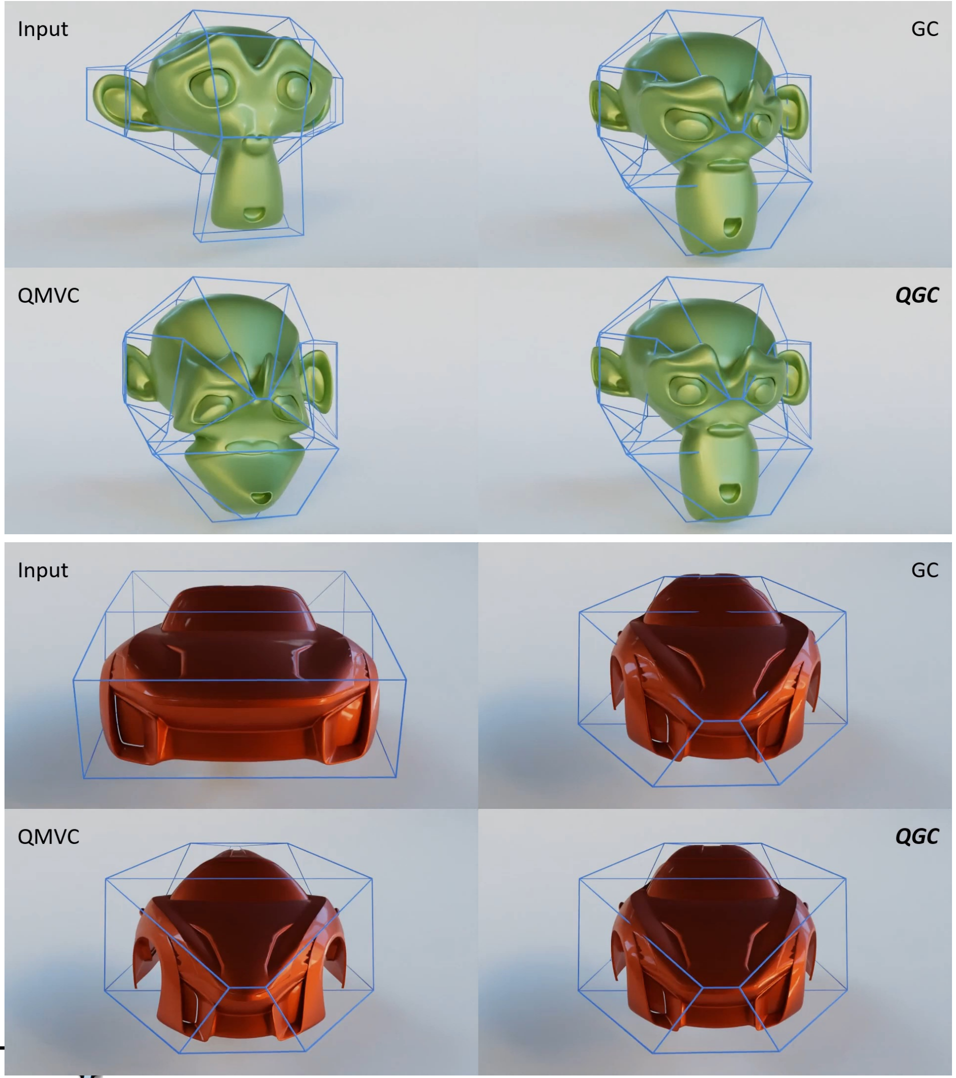

Follow-ups of GC

- High-order cages

Polynomial 2D Green Coordinates for Polygonal Cages

Élie Michel
Adobe Research
France
emichel@adobe.com

Jean-Marc Thiery
Adobe Research
France
jthiery@adobe.com

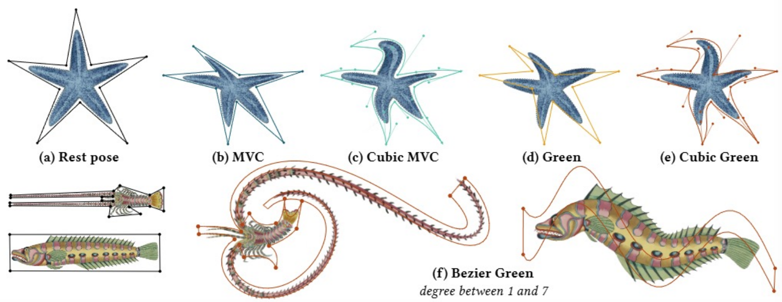

Closed-form Cauchy Coordinates and Their Derivatives for 2D High-order Cages

SHIBO LIU, University of Science and Technology of China, China
LIGANG LIU, University of Science and Technology of China, China
XIAO-MING FU*, University of Science and Technology of China, China

We propose closed-form Cauchy coordinates and their derivatives for 2D closed high-order input cages composed of arbitrary-order polynomial curves. Our coordinates facilitate the transformation of input polynomial curves into output curves of any desired polynomial order. Central to our derivation is the creative use of the residue theorem with the logarithmic function to obtain the integral of a rational polynomial required for extending the classical 2D Cauchy coordinates to high-order input cages. Our coordinates enable smooth cage-aware angle-preserving deformations, and the derivatives allow for point-to-point deformation. Moreover, our derivation can be extended to the input cages with rational polynomial curves. Through various 2D deformations, we demonstrate how users can intuitively manipulate Bézier control points to achieve desired deformations easily.

CCS Concepts: • **Computing methodologies → Shape modeling.**

Additional Key Words and Phrases: Cauchy coordinates, Coordinate derivatives, 2D polynomial coordinates, High-order cages

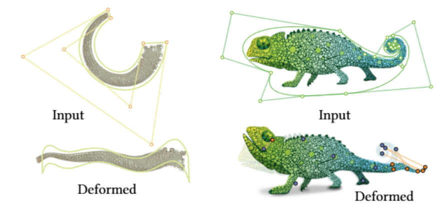

Fig. 1. Deformation via our coordinates and their derivatives. Upper: input images and cubic cages. Bottom: cage-based deformation from cubic to 7th-order cages (left) and point-to-point deformation (right).

Special Section on CAD/Graphics 2025

Polynomial 3D Green coordinates and their derivatives for linear cages

Xiongyu Wu, Shibo Liu, Xiao-Ming Fu *
School of Mathematical Sciences, University of Science and Technology of China, Hefei, Anhui, PR China

ARTICLE INFO

Keywords:
Polynomial 3D Green coordinates
Coordinate derivatives
Cage-based deformation
Variational shape deformation

ABSTRACT

We derive closed-form expressions for polynomial Green coordinates and their derivatives for 3D linear cages. The keys to our derivation are the integrals of polynomials divided by Euclidean distance over a triangle and their derivatives. We demonstrate the usefulness of our polynomial 3D Green coordinates and derivatives on cage-based and variational shape deformations. In cage-based deformation, the coordinates enable deformation from linear polygons of the input cage to polynomial surfaces of any order, allowing users to perform intuitive deformations with a small number of input parameters. In variational deformation, the coordinates and derivatives form a smooth deformation subspace, allowing for the realization of nonlinear shape optimization.

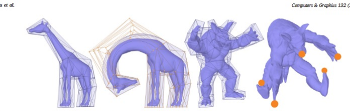

Fig. 2. Left: cage-based deformation using our polynomial 3D Green coordinates, which enable transforming the input cage's linear polygons to third-order polynomial surfaces. Right: variational deformation in a subspace formed by our polynomial Green coordinates.

$$f_p^{ij}(x) = \int_\Delta \frac{u^i v^j}{|x - y(u,v)|^p}\, dudv$$

Follow-ups of GC

- From Green Coordinates to Somigliana Coordinates [Chen et al. 2023]

Green coordinates (GC)

PDE:

$$\Delta \boldsymbol{u} = \boldsymbol{0}$$

Fundamental solutions:

$$G(\boldsymbol{y}, \boldsymbol{x}) = \begin{cases} -\dfrac{1}{4\pi r}, & d = 3, \\ \dfrac{1}{2\pi}\log(r), & d = 2. \end{cases}$$

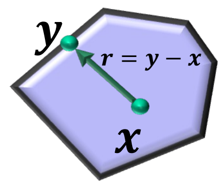

Boundary reformulation:

$$\boldsymbol{u}(\boldsymbol{x}) = \int_{\partial\Omega} \left[\boxed{\nabla_{\boldsymbol{n}} G(\boldsymbol{y}, \boldsymbol{x})}\, \boldsymbol{u}(\boldsymbol{y}) - G(\boldsymbol{y}, \boldsymbol{x})\, \boxed{\nabla_{\boldsymbol{n}} \boldsymbol{u}(\boldsymbol{y})}\right] \mathrm{d}\sigma_{\boldsymbol{y}}$$

$$\boldsymbol{u}(\boldsymbol{x}) = \boldsymbol{x}$$

$$\{\phi_i(\boldsymbol{x}), \psi_k(\boldsymbol{x})\} \in \mathbf{R}$$

Follow-ups of GC

- From Green Coordinates to Somigliana Coordinates [Chen et al. 2023]

Green coordinates (GC)

PDE:

$$\Delta \boldsymbol{u} = \mathbf{0}$$

Fundamental solutions:

$$G(\boldsymbol{y},\boldsymbol{x}) = \begin{cases} -\dfrac{1}{4\pi r}, & d = 3, \\ \dfrac{1}{2\pi}\log(r), & d = 2. \end{cases}$$

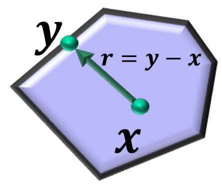

Boundary reformulation:

$$\boldsymbol{u}(\boldsymbol{x}) = \int_{\partial\Omega} \left[\boxed{\nabla_{\boldsymbol{n}} G(\boldsymbol{y},\boldsymbol{x})}\,\boldsymbol{u}(\boldsymbol{y}) - G(\boldsymbol{y},\boldsymbol{x})\,\boxed{\nabla_{\boldsymbol{n}}\boldsymbol{u}(\boldsymbol{y})}\right] \mathrm{d}\sigma_{\boldsymbol{y}}$$

Somigliana coordinates (SC)

$$\Delta \boldsymbol{u} + \frac{1}{1-2\nu}\nabla(\nabla\cdot\boldsymbol{u}) = \mathbf{0}$$

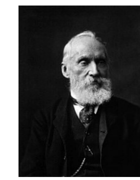

Lord Kelvin

$$\mathcal{K}(\boldsymbol{x},\boldsymbol{y}) = \begin{cases} \frac{a-b}{r}\boldsymbol{I} + \frac{b}{r^3}\boldsymbol{r}\boldsymbol{r}^t, & d = 3, \\ (b-a)\log(r)\boldsymbol{I} + \frac{b}{r^2}\boldsymbol{r}\boldsymbol{r}^t, & d = 2. \end{cases}$$

$$\boldsymbol{u}(\boldsymbol{x}) = \int_{\partial\Omega} \left[\boxed{\mathcal{T}(\boldsymbol{y},\boldsymbol{x})}\,\boldsymbol{u}(\boldsymbol{y}) + \mathcal{K}(\boldsymbol{y},\boldsymbol{x})\,\boxed{\boldsymbol{\tau}(\boldsymbol{y})}\right] \mathrm{d}\sigma_{\boldsymbol{y}}$$

Carlo Somigliana

$$\boldsymbol{u}(\boldsymbol{x}) = \boldsymbol{x}$$

$$\{T_i(\boldsymbol{x}), K_k(\boldsymbol{x})\} \in \mathbf{R}^{d\times d}$$

Follow-ups of GC

- $T_i(\boldsymbol{x})$ and $K_k(\boldsymbol{x})$ are not rotationally invariant!
  - Typical remedy: corotational formulation
- Online computation of deformation

$$\tilde{\boldsymbol{x}}(\boldsymbol{x}) = \left(\sum_i R_i T_i(\boldsymbol{x}) R_i^t\right)^{-1} \left[\sum_i R_i T_i(\boldsymbol{x}) R_i^t \tilde{\boldsymbol{v}}_i + \sum_k R_k K_k(\boldsymbol{x}) R_k^t \tilde{\boldsymbol{\tau}}_k\right]$$

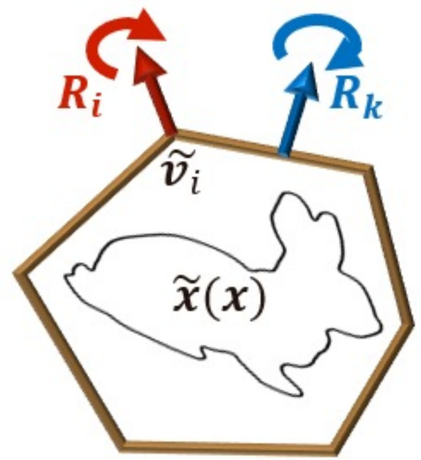

Estimate $\{R_k, \lambda_k, \eta_k\}$ for each boundary facet

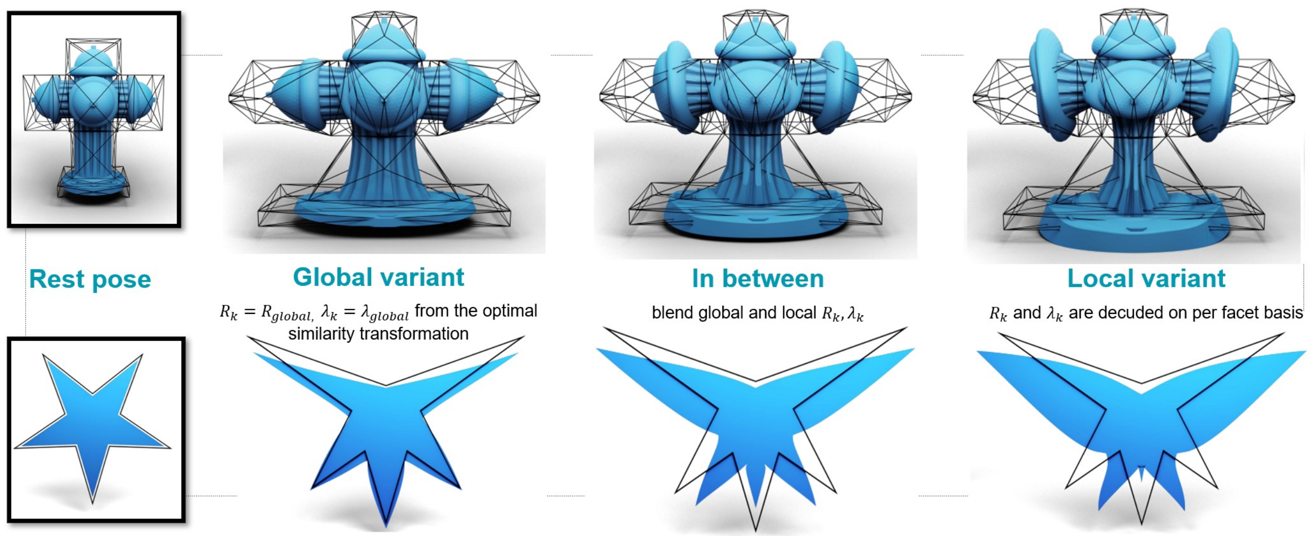

Follow-ups of GC

- Control over the volumetric behavior

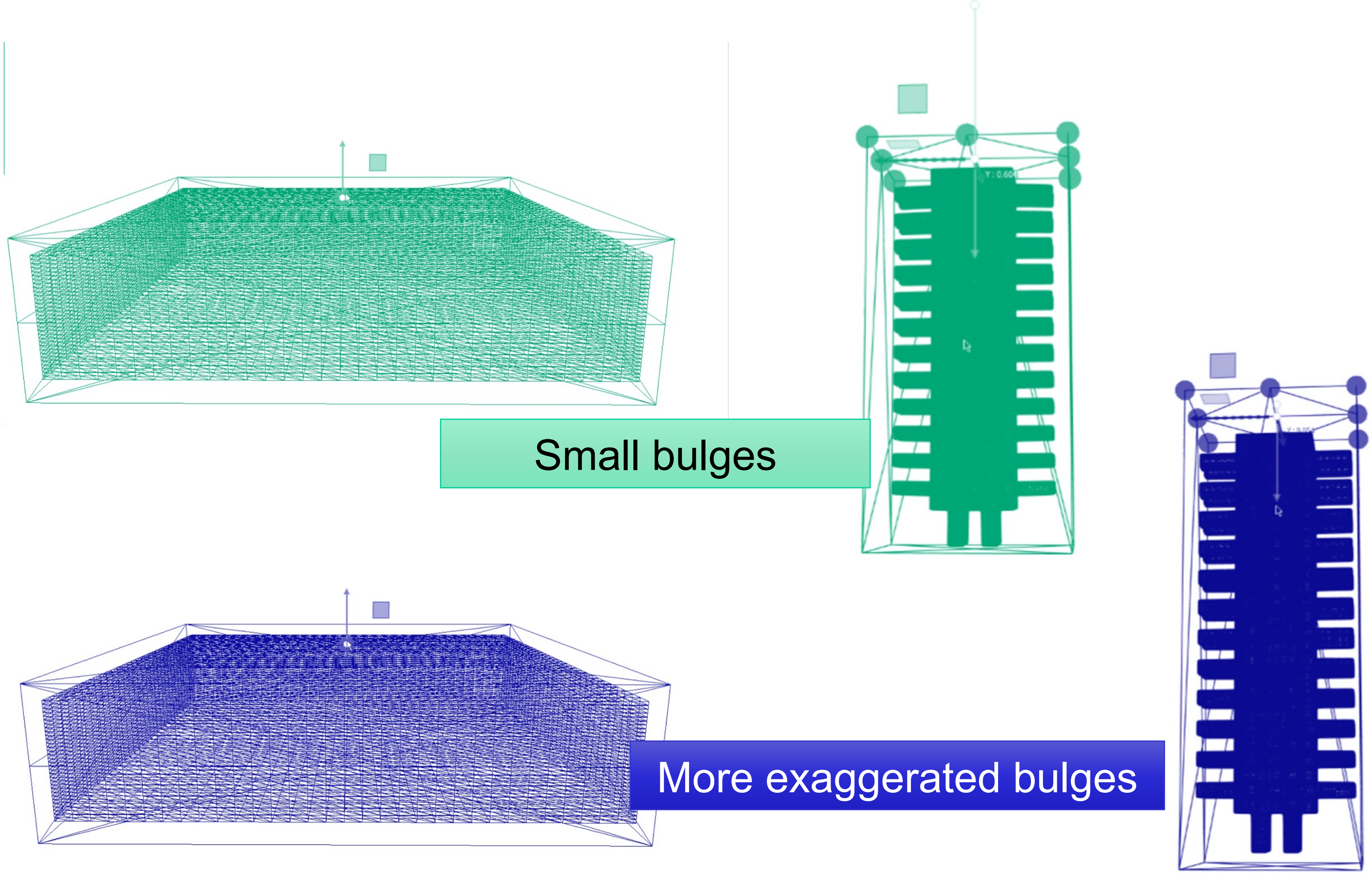

Follow-ups of GC

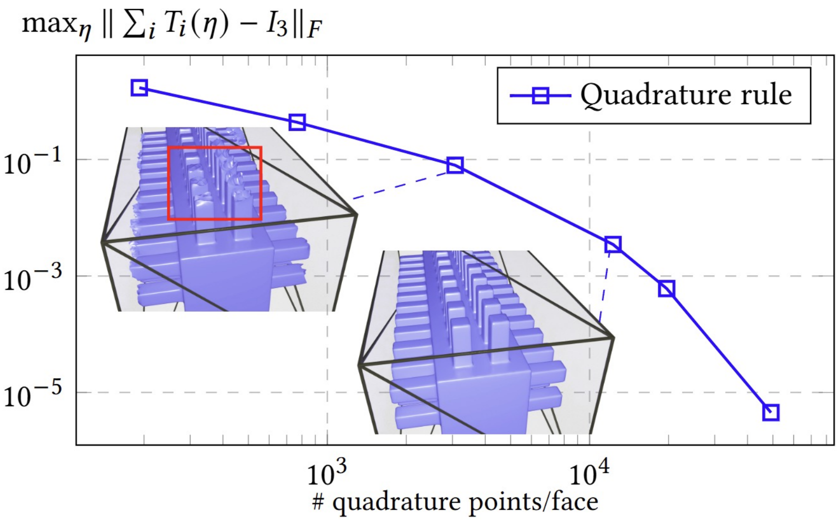

Follow-ups of GC

- Closed-form expression for SC

$$K_t(\eta) = \frac{b}{\lambda_2}\underbrace{H_\eta(\bar{\psi}_t)(\eta)}_{\text{Eq. (13)}} - \frac{a}{\lambda_1}\psi_t(\eta) I_3 \tag{49}$$

$$T^t_{t^i}(\eta) = \frac{2bd_t}{\lambda_1}\underbrace{H_\eta\left(\psi_t^i\right)(\eta)}_{\text{Eq. (46)}} - \frac{a}{\lambda_1}\phi^t_{t^i}(\eta) I_3 - \frac{a-2b}{\lambda_1}\left[n_t \underbrace{\nabla_\eta^T(\psi_t^i)}_{\text{Eq. (45)}} - \underbrace{\nabla_\eta(\psi_t^i) n_t^T}_{\text{Eq. (45)}}\right].$$

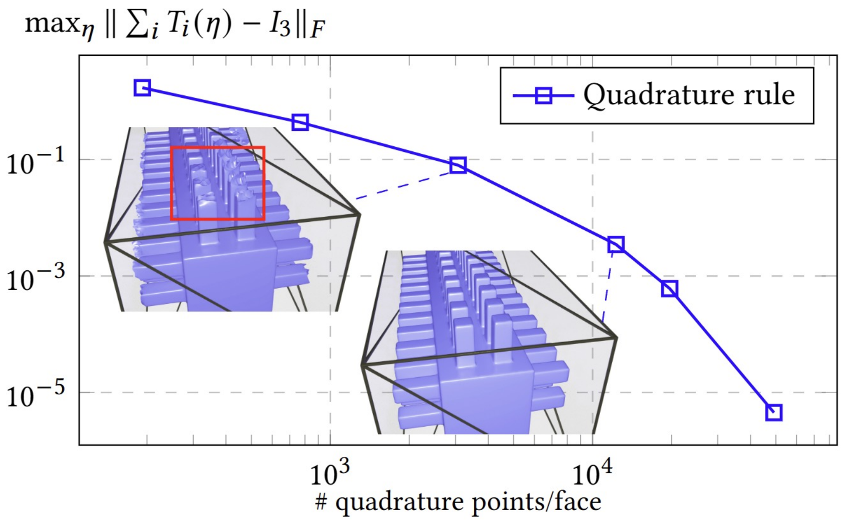

Follow-ups of GC

- Closed-form expression for SC

$$K_t(\eta) = \frac{b}{\lambda_2} \underbrace{H_\eta(\bar{\psi}_t)(\eta)}_{\text{Eq. (13)}} - \frac{a}{\lambda_1}\psi_t(\eta) I_3 \qquad (49)$$

$$T^t_{t^i}(\eta) = \frac{2bd_t}{\lambda_1} \underbrace{H_\eta\left(\psi^i_t\right)(\eta)}_{\text{Eq. (46)}} - \frac{a}{\lambda_1}\phi^t_{t^i}(\eta) I_3 - \frac{a-2b}{\lambda_1}\left[n_t \underbrace{\nabla^T_\eta(\psi^i_t)}_{\text{Eq. (45)}} - \underbrace{\nabla_\eta(\psi^i_t)}_{\text{Eq. (45)}} n^T_t \right].$$

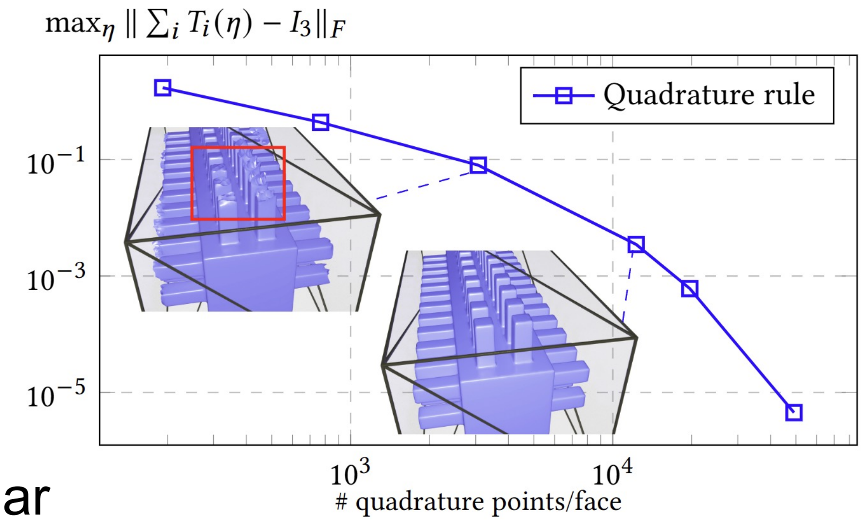

- Biharmonic Coordinates for 3D triangular cages [Thiery et al. 2024]

$$\Delta^2 \boldsymbol{u} = \boldsymbol{0}$$

$$\boldsymbol{u}(\boldsymbol{x}) = \int_{\partial\Omega} [\boldsymbol{u}(\boldsymbol{y}) \nabla_{\boldsymbol{n}} G(\boldsymbol{y},\boldsymbol{x}) - G(\boldsymbol{y},\boldsymbol{x}) \nabla_{\boldsymbol{n}} \boldsymbol{u}(\boldsymbol{y}) + \Delta\boldsymbol{u}(\boldsymbol{y}) \nabla_{\boldsymbol{n}} \bar{G}(\boldsymbol{y},\boldsymbol{x}) - \bar{G}(\boldsymbol{y},\boldsymbol{x}) \nabla_{\boldsymbol{n}} \Delta\boldsymbol{u}(\boldsymbol{y})] \, \mathrm{d}A_{\boldsymbol{y}}$$

$$\begin{cases} G(\boldsymbol{y},\boldsymbol{x}) = -\dfrac{1}{4\pi r} \\ \bar{G}(\boldsymbol{y},\boldsymbol{x}) = -\dfrac{r}{8\pi} \end{cases}$$

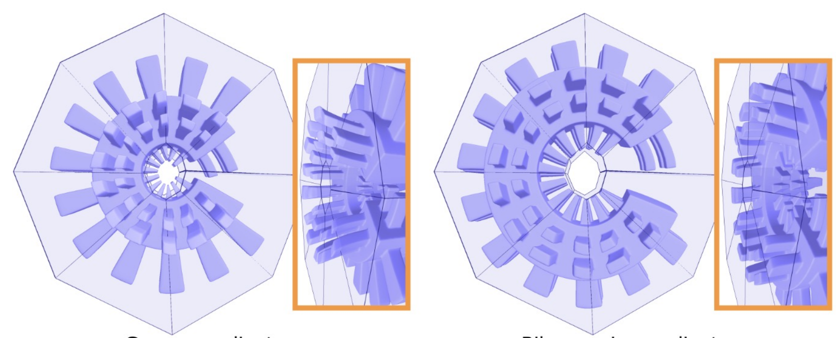

Green coordinates Biharmonic coordinates

Conform better to Dirichlet or Neumann boundary conditions

GBC in Practice

High-res Cage Deformation

- Comparison of most relevant coordinate types
  - They all look similar!

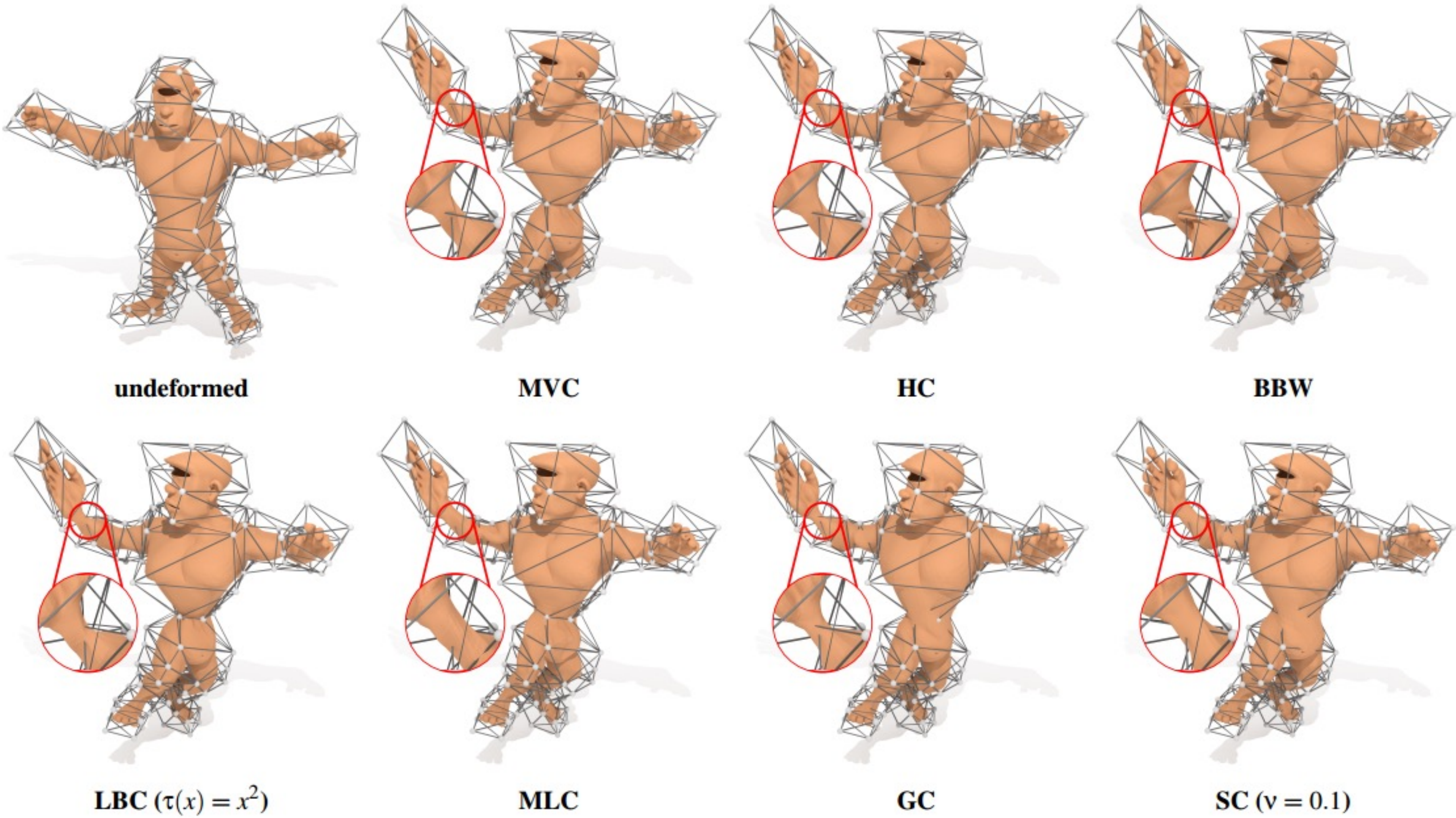

Other issues

- Issues with low-res cages
  - The deformation is more global
  - Hard to achieve intuitive, fine-scale control
- Issues with high-res cages
  - Loses the flexibility of editing
  - Dense matrices need to be stored and transferred
  - Long precomputation time
  - Slow matrix-vector product

$$\begin{pmatrix} \lambda_{11} & \cdots & \lambda_{1N_C} \\ \vdots & \ddots & \vdots \\ \lambda_{N_V1} & \cdots & \lambda_{N_VN_C} \end{pmatrix} \begin{pmatrix} {c'}_1 \\ \vdots \\ {c'}_{N_C} \end{pmatrix} = \begin{pmatrix} {x_1}' \\ \vdots \\ {x_{N_V}}' \end{pmatrix}$$

Precomputed, (#cage_verts, #mesh_verts)

Alternatives: Kelvinlets [de Goes et al. 2017, 2018]

Regularized Kelvinlets

Sculpting Brushes based on
Fundamental Solutions of Elasticity

Fernando de Goes
Pixar Animation Studios

Doug L. James
Pixar Animation Studios
Stanford University

Regularized Kelvinlets

Sculpting Brushes based on
Fundamental Solutions of Elasticity

Fernando de Goes
Pixar Animation Studios

Doug L. James
Pixar Animation Studios
Stanford University

Dynamic Kelvinlets

Secondary Motions based on
Fundamental Solutions of Elastodynamics

Fernando de Goes
Pixar Animation Studios

Doug L. James
Pixar Animation Studios, Stanford University

Dynamic Kelvinlets

Secondary Motions based on
Fundamental Solutions of Elastodynamics

Fernando de Goes
Pixar Animation Studios

Doug L. James
Pixar Animation Studios, Stanford University

Alternatives: Curvenet [de Goes et al. 2022]

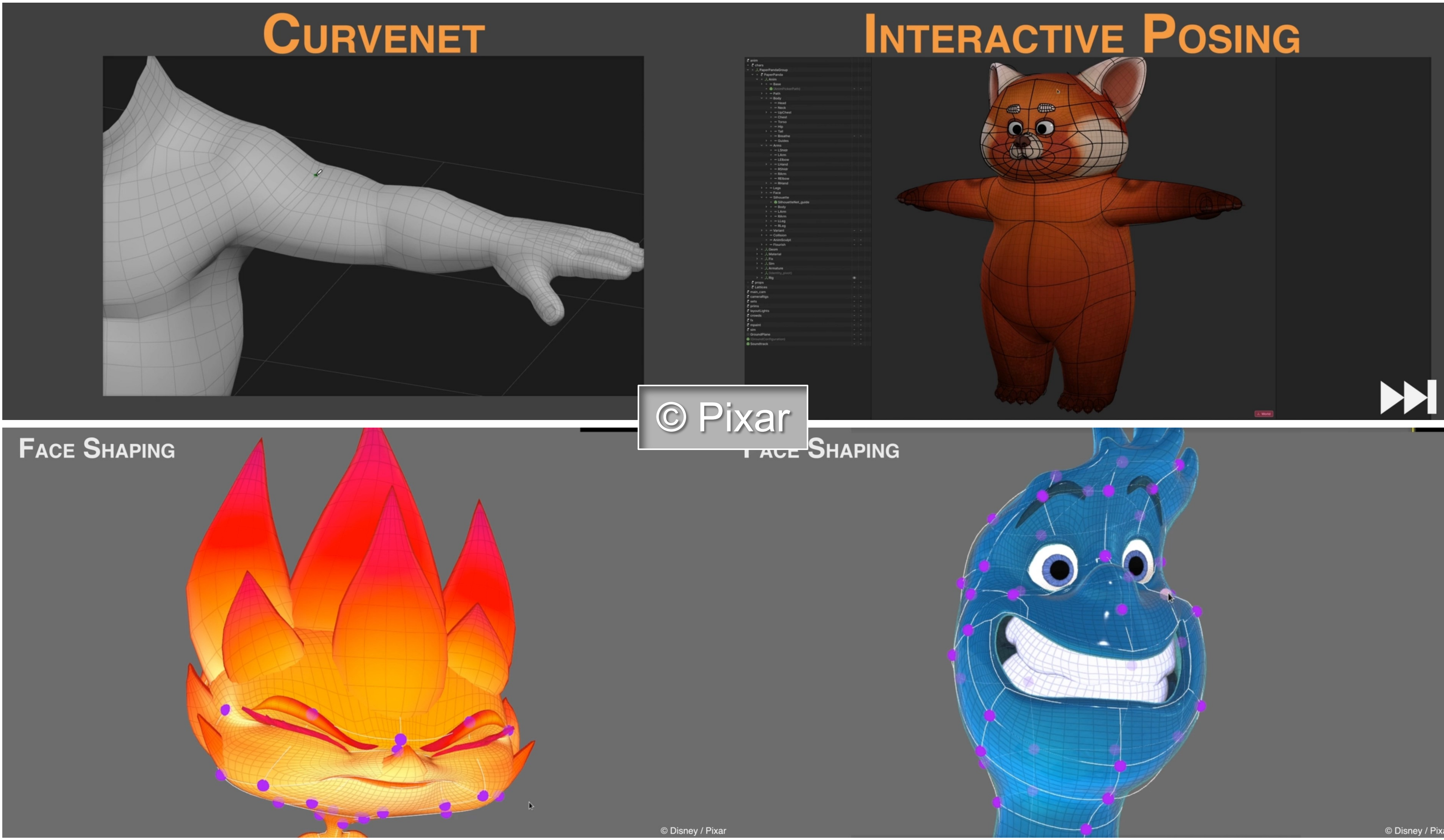

Thanks!